[Journal of the Faculty of Science, Hokkaidô University, Japan, Ser. II, Vol. V, No. 3, 1958]

Visco-elastic Properties of Snow and Ice in Greenland Ice Cap.*

Ukichiro NAKAYA

(Received July 1958)

Abstract.

This is a part of the projects of SIPRE expedition to Greenland in the summer of 1957. A newly designed visco-elastic meter of portable type was brought to Greenland, and the ice samples taken from the ice tunnel were examined by the sonic method at Tuto. Similar experiments were carried out with respect to core samples obtained by drilling in the ice cap at Site 2. Snow samples near the surface of ice cap were also examined. The temperature dependency and the frequency dependency of YOUNG's modulus and viscosity were studied in SIPRE cold room with respect to tunnel ice. YOUNG's modulus was calculated from the resonance frequency, and loss factor was measured by damping method. The MAXWELL model was found to be adequate for explaining the viscous behavior of ice and snow, and the coefficient of viscosity was calculated by using MAXWELL model. The activation energy was calculated from $\log \eta - 1/T$ curve, which is a straight line, and it was found that the value of the old ice cap ice was 18.7 Kcal/mol, which is much larger than that of ordinary ice. The relation between YOUNG's modulus and density was obtained for the whole range of snow and ice observable in Greenland ice cap, The whole region is divided into three regions, each of which shows the different elastic nature. In Region I, density being 0.917–0.90, YOUNG's modulus decreases very rapidly when the density deviates slightly from that of pure ice. In Region II, density being 0.90–0.50, the $E-\rho$ relation is expressed by a straight line, $E=(16.4\rho-7.20)\times 10^{11}$. In Region III, density being 0.50–0.25, the YOUNG's modulus decreases in an exponential form $E=C\exp\{-k(0.50-\rho)\}$. k is the "structure factor" and its value is 6.35 in the case of ordinary settled snow. k becomes smaller in the case of wind packed snow, and larger for the granular snow than that of settled snow. The frequency dependency of viscosity calculated by MAXWELL model is negligible, and a simple relation is observed between $\log \eta$ and ρ. $\log \eta$ decreases linearly with decrease in density until the latter reaches 0.55. Below the density 0.50, another linear relationship is observed with the steeper slope. Comparing this result with $E-\rho$ relation, the YOUNG's modulus and viscosity show the similar behavior as the function of density.

* A part of the report of SIPRE expedition to Greenland. Reprinted from SIPRE Research Paper, No. 46, 1958.

§ 1. Introduction.

Since several years ago the problem of the visco-elastic nature of snow and ice has been taken up by many physicists and glaciologists. Among them the works of DE QUERVAIN[1], GLEN[2], GLEN and PERUTZ[3], STEINEMANN[4], GRIGGS and COLES[5], LANDAUER[6], JELLINEK and BRILL[7], may be considered to be up to date and elaborate. They used the static method and measured the stress and strain relation as well as the rate of creep by applying various stresses to the specimen. On the other hand it is also desirable to study the visco-elastic properties of snow and ice by the sonic method, and KUROIWA and YAMAJI[8][9] carried out the experiments of measuring the YOUNG's modulus and viscosity of snow by using transversal vibration method. The results obtained by this method looked to be successful and the author decided to start the visco-elastic investigation of snow and ice in Greenland ice cap by using the similar instrument as theirs.

The investigations were carried out as a part of the projects of SIPRE expedition to Greenland in the summer of 1957. The author brought a newly designed visco-elastic meter of portable type to Greenland, and stayed at Tuto, 14 miles inland of Thule, and at Site 2 for about 40 days. Site 2 is 220 miles east of Thule, and near 78°N latitude and 7,000 feet altitude. At Tuto the experiments were done with respect to the samples taken from the wall of the ice tunnel, which had been dug into the edge of ice cap near Tuto. At Site 2 the investigation of the visco-elastic properties of snow and ice were done for the samples taken from various depths of ice cap.

After finishing these experiments, some samples of tunnel ice were brought back to SIPRE laboratory in Wilmette, Ill., by the aid of dry ice, and they were studied more in detail in the cold room of SIPRE. The results of all these experiments will be described in this report.

§ 2. Principle of measuring the visco-elastic nature of snow and ice by vibration method.

The principle of measuring YOUNG's modulus is based on the resonance vibration of the sample which is made in the form of

a rectangular bar. The solution of the lateral vibration of a bar was obtained by LORD RAYLEIGH[10] for the case of elastic vibration without internal viscosity. The frequency of the vibration is

$$f = \frac{kbm^2}{2\pi l^2} ,$$

where l is the length of the bar, b the velocity of sound in the material; that is, $\sqrt{E/\rho}$. E is the YOUNG's modulus and ρ the density of the material. m is an abstract number and its value is 4.730 for the fundamental tone, 7.853 for the first harmonics, and so on. k is the radius of gyration of the section about an axis perpendicular to the plane of bending, and $k^2=h^2/12$ in the case of a rectangular bar. h is the thickness of the bar, the width being not introduced in this equation. The YOUNG's modulus, therefore, is obtained for a rectangular bar by eq. (1).

$$E = \frac{48\pi^2 l^4 \rho}{m^4 h^2} f^2 \qquad \text{c. g. s.} \qquad (1)$$

In the case of plastic material the internal viscosity is effective, and the energy dissipates due to the phase lag of the strain behind the stress. The stress-strain relation is expressed in a form of complex numbers, which is studied in detail in the field of high polymers[11]. When the stress σ undergoes a harmonic motion with the angular frequency ω, the strain γ lags behind the stress by the loss angle δ.

$$\sigma = \sigma_0 \sin \omega t ,$$

$$\gamma = \gamma_0 \sin (\omega t - \delta) .$$

The stress-strain relation is conviniently expressed with complex numbers.

$$\sigma^* = G^* \gamma^* . \qquad (2)$$

G^*, which corresponds to YOUNG's modulus in the case of purely elastic materials, is called a complex shear modulus.

$$G^* = G_1 + iG_2 . \qquad (3)$$

The real part G_1 is called a storage modulus and is connected to the elasticity of the material. The imaginary part G_2, a loss

modulus, is a constant related to the internal friction. The dissipated energy is expressed by tan δ, which is called loss factor or mechanical loss.

$$\tan\delta = G_2/G_1 \,. \tag{4}$$

The loss factor tan δ is measured experimentally and there is no problem about its nature, but any attempt to relate this loss factor to the internal viscosity must be accompanied by the introduction of some model, which is of an artificial nature. The relation between the loss factor and the viscosity η is different for different models employed.

The simplest model which expresses the retarded elastic behavior is the VOIGT model; a spring with E_1 and a dashpot with η_1 are combined in parallel. The equation of motion is

$$\dot{\gamma} + \frac{1}{\tau}\gamma = \frac{1}{\eta_1}\sigma \,, \tag{5}$$

in which $\tau = \eta_1/E_1$ is the retardation time. The solution is

$$G^* = G_1 + iG_2 = E_1 + i\omega\eta_1 \,. \tag{6}$$

G_1 is the YOUNG's modulus of the spring, and G_2 is directly proportional to the viscosity of the dashpot. The loss factor is proportional to the viscosity.

$$\tan\delta = \omega\eta_1/E_1 \,. \tag{7}$$

For the MAXWELL model which is a combination of a spring with E_2 and a dashpot with η_2 in series, the equation of motion is

$$\dot{\sigma} + \frac{1}{\tau'}\sigma = E_2\dot{\gamma} \,, \tag{8}$$

in which $\tau' = \eta_2/E_2$ is the relaxation time. The solution is

$$G^* = E' + i\omega\eta' \,,$$

$$E' = E_2\frac{\omega^2\tau'^2}{1+\omega^2\tau'^2} \,, \qquad \eta' = \frac{E_2\tau'}{1+\omega^2\tau'^2} \,,$$

or

$$E' = E_2\left(1+\frac{1}{\omega^2\tau'^2}\right)^{-1}, \qquad \eta' = \frac{1}{\eta_2}\frac{E_2^2}{\omega^2}\left(1+\frac{1}{\omega^2\tau'^2}\right)^{-1}. \tag{9}$$

$$\tan\delta = E_2/\omega\eta_2 \,. \tag{10}$$

In this case the loss factor is inversely proportional to the viscosity, being contrary to the case of VOIGT model. The interpretation of the mechanical loss in terms of viscosity is quite different for different models. On the other hand, the term representing the elasticity is almost the same for the two models. The equations (6) and (9) show that the equivalent YOUNG's modulus is the same as that of the model spring in the case of VOIGT model, and almost the same with some correction in the case of MAXWELL model.

The solution of the lateral vibration of a rectangular bar with damping is obtained by YOSIDA[12]. The vibration attenuates with the damping coefficient λ.

$$A = A_0 e^{-\lambda t} \sin \omega t . \tag{11}$$

λ and ω are expressed by

$$\omega^2 + \lambda^2 = \frac{m^4 h^2 E}{12 l^4 \rho} . \tag{12}$$

In most cases λ^2 can be neglected with respect to ω^2, and (12) becomes (1). The loss factor is expressed by

$$\tan \delta = 2\lambda/\omega . \tag{13}$$

The mode of damping was checked at various temperatures with respect to C 1 and C 2 ices; Table II. The logarithm of amplitude decreases linearly with time; Fig. 1, and the value of λ is determined by the slope of the straight line.

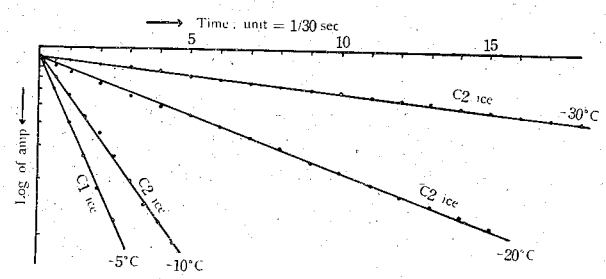

Fig. 1. The mode of damping at various temperatures.

By measuring λ from the oscillogram, $\tan \delta$ is calculated by (13), and the coefficient of viscosity is given by

$$\left.\begin{aligned} \eta_1 &= \frac{E_1 \tan\delta}{\omega} && \text{for VOIGT model} \\ \eta_2 &= \frac{E_2}{\omega \tan\delta} && \text{for MAXWELL model} \end{aligned}\right\} \qquad (14)$$

The viscosity expressed by (14) is that of the model dashpot, and is different for different models. So long as not much knowledge is obtained about the mechanism of dissipation of energy, the value of viscosity thus obtained has little physical meaning, but it will serve as a clue for the study of the mechanism of energy dissipation. The value of tan δ, which expresses the mechanical loss due to internal viscosity, is that determined experimentally and is free from the type of model used. In this paper, therefore, tan δ was mostly used for the description of the viscous nature of the sample. The dissipated energy ΔW due to visco-elastic loss in the material is

$$\Delta W = \pi \tan\delta \, G_1 \gamma_0^2 . \qquad (15)$$

G_1 is the YOUNG's modulus itself in the case of VOIGT model and approximates to it in the MAXWELL model. For the given amplitude tan δ is exactly or nearly proportional to the amount of dissipated energy per cycle.

§ 3. Experimental method for the determination of visco-elastic properties of snow and ice.

The schematical diagram of the instrument used in Greenland is shown in Fig. 2. The sample of snow or ice S is cut in the shape of a rectangular bar, and is supported on two strings stretched horizontally. The position of the string must coincide with the nodal point of the vibration, but a deviation of a few mm does not affect the result sensibly. The nodal point is 0.22 l from each end in the case of fundamental vibration. A small thin iron plate is frozen to each end of the bar; I_1 and I_2. This plate is the thinner the better, and the vibrating plate of telephone receiver is used. The ordinary CR oscillator is connected to the exciting coil C_2 through an amplifier and this gives rise to the forced oscillation of the bar. By the use of a variable condenser the frequency of the exciting current is changed continuously. When this frequency coincides with that of the resonance vibration of

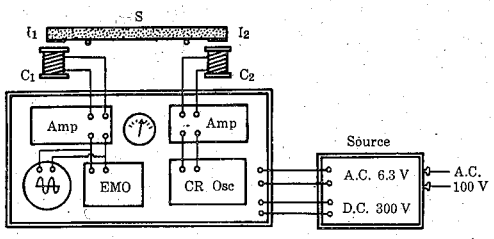

Fig. 2. The schematical diagram of the portable visco-elastic meter.

the bar, the induced current in coil C_1 due to the vibration of iron plate I_1 becomes maximum. This induced current is amplified and recorded on an electromagnetic oscillograph. Type 5-118 of Consolidated Engineering Corporation with paper speed of 3 inches per second was used for this purpose. As the time mark 60 cycles of the generator was used. An additional cathode ray oscilloscope was provided for the purpose of eye observation of the wave form and the amplitude. The resonance frequency was measured on the dial which had been calibrated with the 60 cycles of the generator.

In this series of experiments only the fundamental vibration was measured. In the case of soft snow sometimes the second harmonic takes place, which is $4\frac{\lambda}{2}$. In this case the supporting string is near the loop of the wave, and the string easily cuts into the snow sample. If it once happens the sample is damaged. The forth harmonic $6\frac{\lambda}{2}$ is also liable to occur. The position of the string is near the nodal point in this case, and sometimes this is mistaken as the fundamental vibration. The harmonics of odd number, $3\frac{\lambda}{2}$ or $5\frac{\lambda}{2}$, is difficult to occur in the case of soft snow.

After the resonance frequency was measured, the exciting current was short-circuitted and the mode of damping was recorded on the oscillograph. Several samples of these oscillograms are shown in section 10. The amplitute decreases exponentially with time. The energy loss is calculated from the slope of the straight line shown in Fig. 1. In most cases the attenuation constant was

calculated by measuring the time required for the diminution of the amplitude to 1/3 of the initial value. The dimension of samples was usually, except the case of soft snow, l~20–25 cm, h~5–10 mm, b~2 cm, and the resonance frequency was between about 200 and 300. For the study of frequency dependency the frequency was varied in the range of 150 and 650.

§ 4. Visco-elastic properties of tunnel ice.

Visco-elastic properties of ice samples taken from various positions of the ice tunnel were measured by the sonic method. The samples contained air bubbles and air columns captured in the ice. Five kinds of ice samples were tested in the room constructed in the tunnel, where the air temperature was almost constant at nearly −5°C. The temperature, however, sometimes went up to −4°C or so. Eighteen data, T 1 through T 18, were tested. The specification of samples used in this experiment is shown in Table I. Some of the samples were brought back to SIPRE laboratory

TABLE I. Ice samples used in the tunnel experiments.

No.	ρ	nature of ice	Butkovitch notation*
A 1	0.916	superimposed ice	MP 5
B 1	0.905–0.908	air columns & elongated bubbles	MP 2
D	0.9125	air bubbles & dirt bands	MP 4
E 1	0.910	many small bubbles	MP 4
E 2	0.913	" " "	MP 4

* His paper on the mechanical properties of tunnel ice will appear shortly in SIPRE report.

TABLE II. Ice samples used in the SIPRE Laboratory.

No.	ρ	nature of ice	Butkovitch notation
I	0.917	commercial ice without bubbles	—
A 2	0.915	superimposed ice	MP 5
B 2	0.910	air columns and elongated bubbles	MP 2
C 1	0.911	many very small bubbles; 680′ from entrance of tunnel	
C 2	0.910	" " " " " " " " "	

in Wilmette, Ill., by the aid of dry ice, and more detailed investigations were carried out in the cold room at various temperatures. The samples used in the experiment at SIPRE are enumerated in Table II.

A1 and A2 are the superimposed ice, which is caused by the avalanche of relatively new snow. This is not the ice inside of ice cap and is found near the entrance of the tunnel. It contains a few small bubbles and is fairly transparent and looks bluish *in situ*. The density is nearly that of pure ice. A microphotograph of A2 ice is reproduced in Fig. 3*, which is taken under crossed polaroids. B1 and B2 belong to one type which is characterized by the presence of air columns and elongated bubbles, which are well oriented in one direction. One example of B2 ice is shown in Fig. 4. Ice samples of this kind show sometimes diversified nature even if they are taken from one location. The density varies between 0.905 and 0.910. For the detailed investigation, this type must be classified into several subgroups. E1 and E2 were taken at one spot, the former having been taken horizontally and the latter vertically. This ice contained many small bubbles and showed a milky appearance with slightly bluish tint. The bubbles are not spherical in shape and show a tendency of orientation in one direction. Judging from the shape and size of the bubbles, E ice is considered to be much older than B ice. In the region of E ice, sometimes fine silt or clay particles are observed in the ice, being arranged in the form of bands. This ice with dirt bands is called D ice. The density of D ice is nearly the same as that of E ice, but YOUNG's modulus shows a high value. C1 and C2 were taken at the spot 680 feet from the entrance of the ice tunnel. As shown in Figs. 5 and 6, the bubbles are very small and abundant in number. Some of them are seen on the grain boundaries, but most of them are captured in the grain. The general appearance of bubble is ovoidal and a slight tendency of orientation is observed.

The YOUNG's moduli of these samples are plotted against density in Fig. 7. The points are scattered in a wide range showing that the amount and size of air bubbles affect the elastic property in various ways. The general tendency, however, is observed that

* The number of Figures in Gothic means the picture in the Plate.

the YOUNG's modulus decreases linearly with the increase of air void. The interesting point is that a slight decrease in density results in a rapid decrease in YOUNG's modulus. This point is important in the discussion of the relation between YOUNG's modulus and density for the wide range of ice samples taken from the ice cap; Fig. 25. The samples of E ice marked by 5 and 7 in Fig. 7 were cut from the sample taken horizontally, and those 8 and 9 were taken vertically. The latter shows much higher value of E than the former. The similar effect, however, is not observed in the case of B1 ice. From one block of B1 ice, which shows a marked orientation of elongated air bubbles, three kinds of samples were made. The direction of orientation of bubbles was taken in x, y and z directions respectively. The data are shown by white circles 11 through 16, and no marked anisotropy is observed in this case. The dark circles 17 and 18 show the YOUNG's modulus of D ice. This remarkably high value for the ice containing silt particles is considered to promise the study of frozen soil by this sonic method. The data shown by double circles are those otained in SIPRE laboratory.

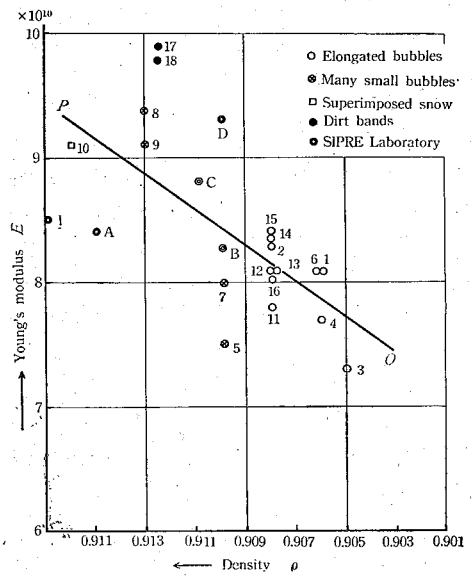

Fig. 7. YOUNG's modulus versus density; tunnel ice.

The viscosity measurement was carried out with respect to 6 samples. One oscillogram of tunnel ice is reproduced in Fig. 29 to show the mode of damping. The mean value of $\tan\delta$ is 0.0344 for B1 ice, 0.0333 for E1 ice and 0.0287 for E2 ice. The data show that the mechanical loss is smaller for higher density of the sample. This point will be discussed again in section 13.

§ 5. Elastic properties of ice samples taken from the deep pit.

In 1954 a pit of 100 feet depth was dug in the ice cap at Site

2. This is called the deep pit. A series of pegs was fixed to the wall at various depths, when this deep pit was made. These pegs are called PA, PB,···, PG. PA is near the surface of ice cap and PG is at the bottom of the pit. The density near the surface is about 0.45 and increases to 0.65 at the bottom. Thin section of samples taken from various depths was made and the structure was studied under a microscope. Microphotographs of four samples are shown in Figs. 8–11. The sample taken from the level of PB is the ordinary settled snow, but some larger grains are mixed; Fig. 8. The grains of snow become larger as the layer goes deeper, and the air space between the grains transforms into a network of air columns. This process will be seen in the series of microphotographs; Figs. 10 and 11. Fig. 11 shows the structure of compacted snow at the bottom of the deep pit, in which the network of air columns is clearly seen. In this stage the snow is still permeable to air, although the general appearance looks like a translucent solid ice.

The experiments at Site 2 were carried out in the cold room, the temperature of which was kept almost constant at −9°C. The wall and ceiling are covered with glass fabrics and refrigeration is made by sending the cold air into this room, which is sucked from the deep level of the ice cap. The YOUNG's moduli of the samples taken from PB–PG layers are measured in this cold room and the results are plotted as the function of density; Fig. 12. Most of the data lie on a straight line, except those of PD and PE. These two layers are a little different in structure from the others, showing the appearance like a compacted granular snow. The microphotograph of PD, Fig. 9, shows this granular nature. It is expected that the compacted snow with granular structure shows the smaller value of YOUNG's modulus compared with that of settled snow with the same density. The result of the experiment agrees with this expectation.

All the samples above mentioned were taken horizontally from the snow wall by a hand auger. For the deeper levels than the bottom of the deep pit, the sample must be taken by drilling. In that case the core is taken vertically. In order to connect the data of deep pit samples to those of core samples, the comparison was made for the samples taken horizontally and vertically at the

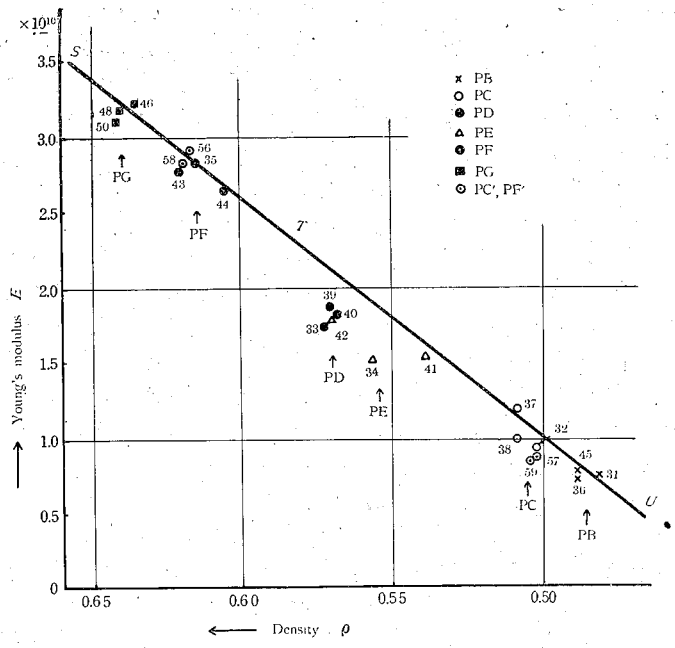

Fig. 12. YOUNG's modulus versus density; samples of deep pit, PC′ and PF′ are two years old.

same spot of PG. The results are shown in Fig. 13, in which the line ST is the portion of the line marked ST in Fig. 12. The vertical sample shows a tendency to be a little larger than the horizontal sample, but the difference may be neglected if we are satisfied with the accuracy of ±5%. In this series of experiments the length of the bar was also changed between 24.9 cm and 14.9 cm, and the thickness between 5.5 mm and 9.9 mm, so that the resonance frequency varied between 210 and 575. The YOUNG's modulus is a function of frequency, and it decreases slightly with the frequency as will be described later

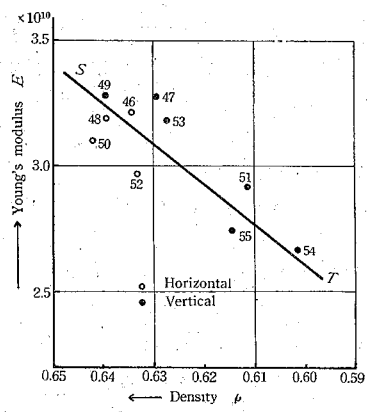

Fig. 13.

Comparison of the samples taken horizontally and vertically at PG; $f=210-575$.

in section 11. Fig. 13 can be interpreted that the effect of frequency also may be neglected if the accuracy is limited within $\pm 5\%$.

The snow is subjected to an intense stress at deep level of the ice cap, and this stress in the sample must be released when the sample is taken out of the wall. It might happen that the elastic nature is different for the newly taken sample and the old sample taken from the same level. At the levels of PF in the deep pit, core samples were taken two years ago and they were left in the core holes until this year. These samples were tested in the same way as the newly taken samples, and the data are plotted in Fig. 12 as PC′ and PF′. These points lie, on the same line, and it is understood that the release of internal stress does not affect the YOUNG's modulus sensibly.

§ 6. Elastic properties of core samples taken by drilling.

Drilling in the ice cap was carried out in 1956 and 1957, and 4 inch core was obtained from various depths. When drilling proceeds deeper than about 80 m, the ice becomes impermeable to air and the network of air columns seen in Fig. 11 transforms into a group of air columns and bubbles. One example is shown in Fig. 14. In a long period of time the air column splits into a series of air bubbles due to the effect of surface energy; Fig. 15. The mechanism of this transformation is described in detail for the case of vacuum figures of columnar shape captured in singel crystals of ice[13]. The mechanism is the same for both cases, the only difference being that the process is much slower in the case of air columns. Proceeding still deeper, the air bubbles become smaller and smaller as the ice is compacted due to its viscous nature. The pressure of the bubble gets higher and higher and LANGWAY[14] measured the mean value of pressure as high as 14 atmospheric pressures. The ice sample taken from the deep layer of ice cap is such a peculiar material as the ice containing numerous infinitesimal air bubbles of high pressure.

The YOUNG's modulus of 1956 and 1957 cores were measured and plotted as the function of density; Fig. 16. In Fig. 16, the full line SU is the line determined by the samples of the deep pit, and is the same as the line SU in Fig. 12. The core samples

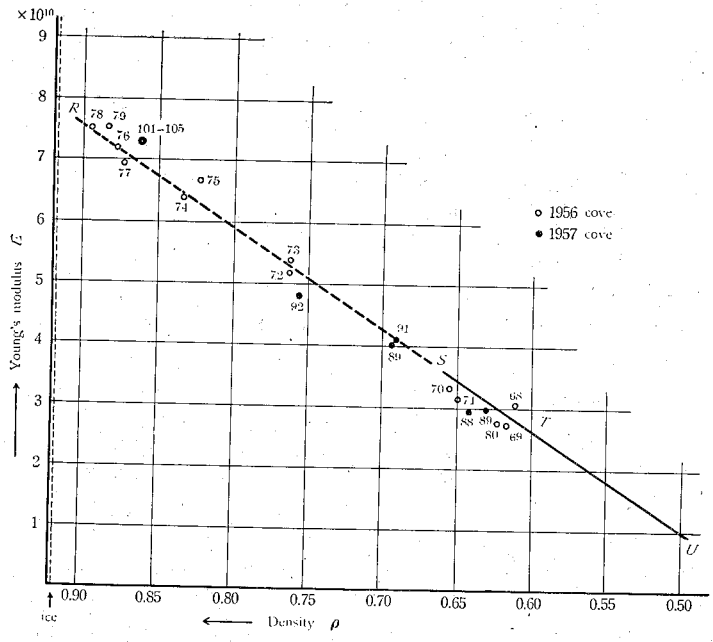

Fig. 16. YOUNG's modulus versus density; 1956 core and 1957 core.

of the density less than 0.65 give the concordant value of YOUNG's medulus as that obtained by using the samples of the deep pit. The most interesting point is that all data obtained for the samples of deeper layers lie on a straight line RS which is the extension of SU. The YOUNG's modulus is a linear function of the density in the wide range of the latter. The empirical formula of this line is

$$E = (16.4\,\rho - 7.20) \times 10^{10} \qquad (16)$$

for the range of ρ between 0.9 and 0.5.

The YOUNG's modulus of pure ice is nearly 9×10^{10}, and the extension of this line to $\rho = 0.917$ gives a much lower value. This point agrees with the phenomenon shown in Fig. 7; the rapid decrease in YOUNG's modulus with the slight decrease in density. The scale of density is quite different for Fig. 7 and Fig. 16. Putting these two regions together, the $E-\rho$ relation is shown in Fig. 17. The lines PQ and RS are transfered from Fig. 7 and Fig.

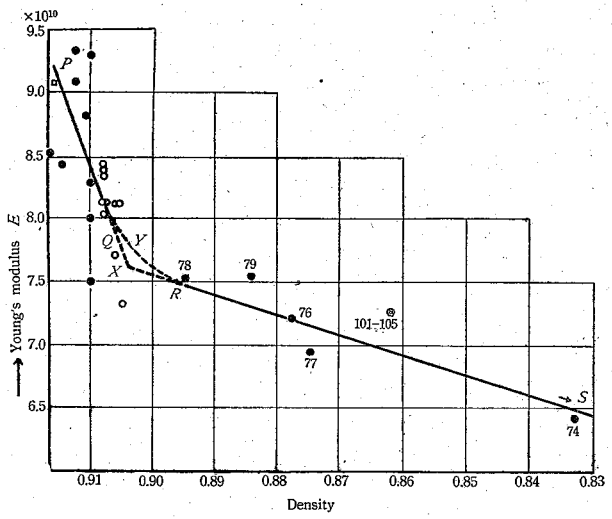

Fig. 17. YOUNG's modulus versus density; tunnel ice and core samples.

16 respectively. It looks as if there is a discontinuity in the slope at X; that is, at the density of about 0.905. It is difficult to figure a mechanism which gives a discontinuous nature in elasticity at such a density as 0.905. The transition from PQ to RS may take the course shown by Y in Fig. 17. In any case the result of experiment shows that the YOUNG's modulus decreases very rapidly when the density deviates slightly from that of pure ice and after $\rho=0.905$ the rate of decrease diminishes remarkably.

There is another way of interpretation of this phenomenon. The nature of tunnel ice may be different qualitatively from that of core samples. The deepest layer, from which the sample is taken, is 155 m from the surface. This ice may be about 300 or 350 years old, but cannot be very old. The tunnel ice, however, can be very old, if the ice near the bottom of the ice cap flows towards the edge of the ice cap. In that case, the elastic nature may be different for these two kinds of ice.

§ 7. Elastic properties of snow near the surface of ice cap.

a) *Vertical distribution of YOUNG's modulus near the surface.*

In 1956 a large trench was made at Site 2 in order to set a

boring machine. The snow wall of this trench has been exposed to the atmosphere for one year, and the surface was etched so that the layer structure of snow cover was made faintly visible. A block of snow about 0.5 m in thickness was cut from this wall, and it was sliced horizontally into 18 sheets. The YOUNG's modulus and density were measured for each of these slices and the vertical distribution was examined. The result is shown in Fig. 18. The density and YOUNG's modulus show a good parallelism, and both values show minimum in the layer of coarse grain and maximum in icy layer.

The relation between YOUNG's modulus and density is shown

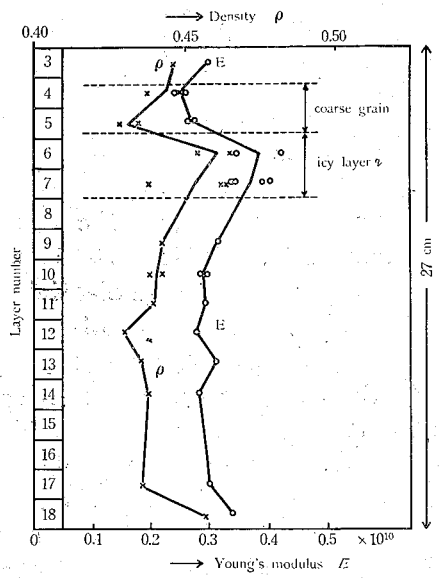

Fig. 18.
Vertical distribution of YOUNG's modulus and density; sample Nos. 3-22.

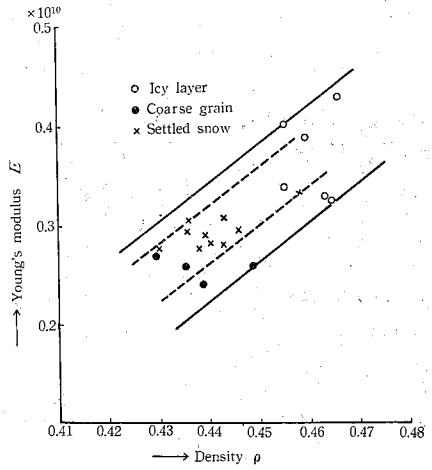

Fig. 19.
YOUNG's modulus versus density; snow near the surface, Sample Nos. 3-22.

in Fig. 19, irrespective of the nature of snow. The points are scattered in a wide range, although the general tendency is a linear relationship between E and ρ. $\Delta E/E$ is about 30 % when all kinds of snow are treated as a whole. As for the ordinary settled snow only, $\Delta E/E$ reduces to nearly 15%. The YOUNG's modulus of snow is considered to be a function of density and structure of snow.

As the action of glaciation of snow proceeds, the YOUNG's modulus will become larger than that of the ordinary settled snow of the same density. When snow becomes granular, the reverse will be the case. This point will be discussed later in detail in Figs. 23 and 24.

b) *The wind packed snow.*

The snow on the surface of ice cap is sometimes packed by the action of wind. The wind packed snow shows a slight increase in density, but the hardness becomes very large. The structure of new wind packed snow is shown in Fig. 20. A portion of snow particles undergo metamorphosis, but some of them still show the original shape of snow crystals. These particles are bonded together and give rise to an increase in the YOUNG's modulus.

c) *Peter snow.*

The snow disaggregated and deposited by the Peter Snow Miller has a high density and becomes fairly hard within a few weeks. This snow is called "Peter snow" for convinience' sake. In the summer of 1956 an accumulation of Peter snow about 1 m in thickness was made and left for one year. Blocks of this one year old Peter snow were cut from this accumulation, and the vertical distribution of the YOUNG's modulus and density were studied. The results are shown in Fig. 22. Both the YOUNG's

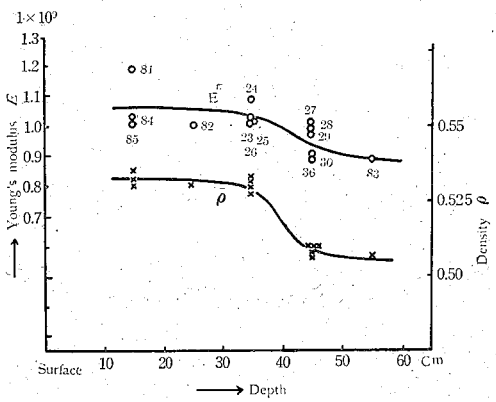

Fig. 22. Vertical distribution of E and ρ in Peter snow of one year old; Sample Nos. 23–30, 81–86.

modulus and the density show high values which correspond to those of the sample taken from the wall PC of the deep pit. They are almost constant to the depth of 40 cm from the surface and become smaller below 40 cm. The structure of Peter snow is shown in Fig. 21. It is interesting to notice that the structure is similar to that of the samples taken from the deep pit.

d) *The relation between YOUNG's modulus and density of snow.*

The YOUNG's modulus and density were measured for various samples of snow; ordinary settled snow, wind packed snow, granular snow and Peter snow. The results are shown in Fig. 23, in which the line TU represents the data obtained for the samples of the deep pit; that is, it is transfered from Fig. 12. The curve VW, which is in an exponential form, is for the ordinary settled snow. The interesting point is that the data for wind packed snow are

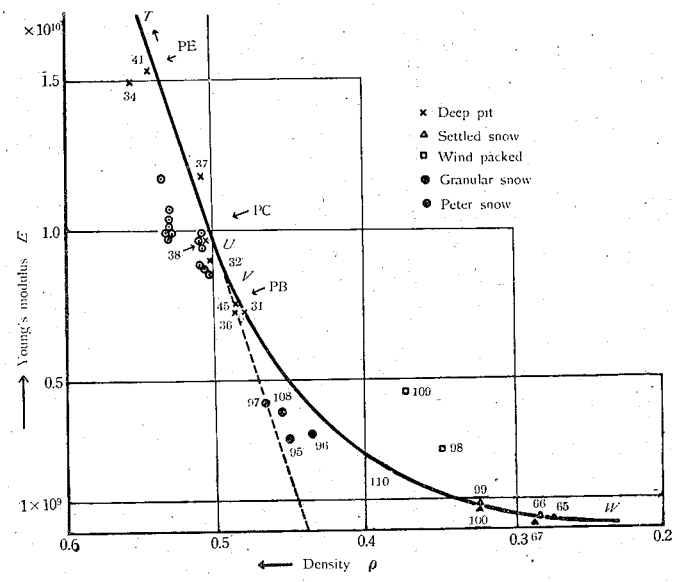

Fig. 23. YOUNG's modulus versus density; snow near the surface of ice cap.

decidedly above this VW line. The YOUNG's modulus of wind packed snow is usually a few times larger than that of the settled snow of the same density. In the case of the granular snow, the contrary is the case. The YOUNG's modulus is not only the func-

tion of density, but it must be influenced by the mode of bonding of particles and possibly by the size distribution. The present result is concordant with this conception.

In order to get a closer insight, the same data are plotted in

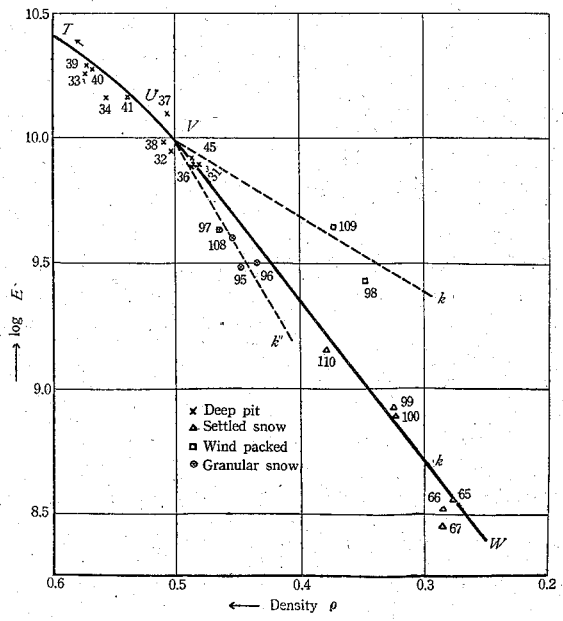

Fig. 24. log $E-\rho$ curve; snow near the surface of ice cap.

the semi-logarithmic scale; Fig. 24. The exponential portion is expressed by the straight line VW in Fig. 24. The empirical formula takes the from

$$E = C \exp\{-k(0.50-\rho)\} \qquad (17)$$

for the range of ρ between 0.50 and 0.25. k is a factor determined by the structure of snow and may be called "structure factor". The structure factor gets lower value when the bonding between particles becomes stronger. In Fig. 24, the structure factor for wind packed snow is k' and for granular snow k''. For the ordinary settled snow k is 6.35 and the empirical formula is

$$\log E = 6.80 + 6.35\,\rho\ . \qquad (18)$$

Up to this stage the structure factor is only a mathematical

expression. It is desirable to correlate this factor to the configuration of snow particles by experiments. For that purpose the examination of the structure of snow by FUCHS' method[15] must be carried out in parallel with this sonic experiment. Once the relation between k and structure of snow is established, this structure factor will be introduced effectively into the mechanics of snow.

The data for Peter snow are also plotted in Fig. 23. They are found close to the data of PC of the deep pit. The so called powder snow observable in Greenland ice cap is difficult to be compacted artificially, but it is compacted in a long period of time under the snow cover due to the weight of snow deposited above this layer. In the case of Peter snow, the compacted state is obtained in a few weeks or few months, which corresponds to that of PC in the deep pit. The time required to get the state of PC by natural compaction is about 20 years. The process of making Peter snow may be considered to shorten the time of 20 years in the natural course to a few weeks or few months.

§ 8. Relation between YOUNG's modulus and density.

Compiling Figs. 7, 12, 16 and 23, the relation between YOUNG's modulus and density is plotted for the whole range of snow and ice observable in Greenland ice cap. Fig. 25 shows that the whole range is divided into three regions, I, II, III. When the density deviates slightly from the pure ice, the YOUNG's modulus decreases rapidly. This is the first part, Region I. This region is called the ice region for the descriptive purpose. The samples of this region were obtained from the ice tunnel. The range of density is between 0.917 and 0.90. The material is almost ice with small air void.

The second part, Region II, covers the range of density between 0.90 and 0.50. The samples of this region are obtained from the wall of the deep pit or the core samples of drilling. The material is the intermediate state of snow and ice, and the general appearance looks like a translucent ice. Most of the samples in this region, however, are still permeable to air. This region will be called the core region. It is remarkable that the relation between YOUNG's modulus and density is expressed by a straight

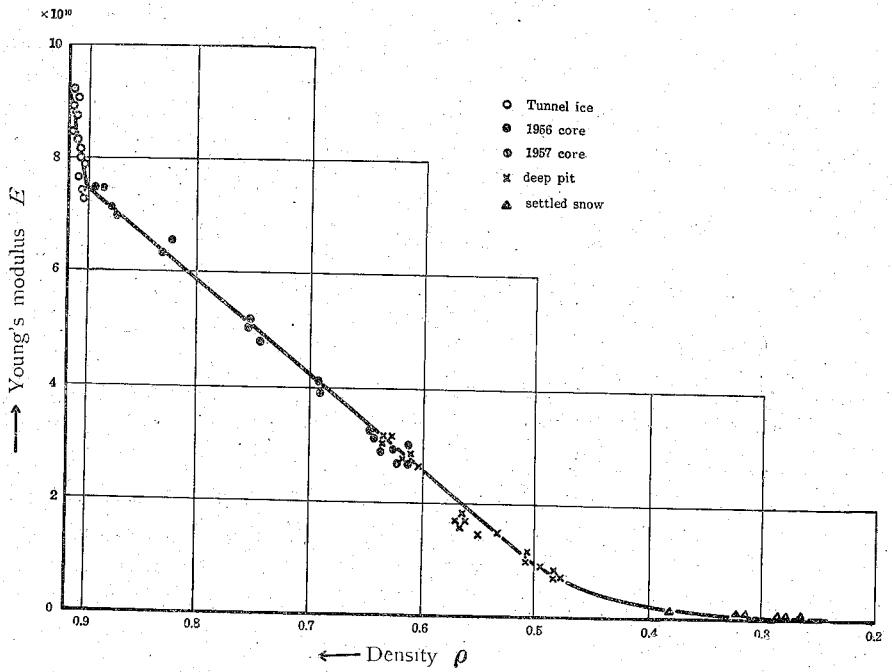

Fig. 25. The relation between YOUNG's modulus and density for the whole range of Greenland ice and snow.

line for the whole range of this core region.

The third part, Region III, is the soft snow near the surface of ice cap, the density ranging between 0.50 and about 0.25. This part will be called the snow region. The samples in this region show a variety in nature, and for the ordinary settled snow the YOUNG's modulus decreases in an exponential form with decrease in density. The data for wind packed snow lie above this exponential curve, and those for granular snow below this curve. The physical interpretation of this $E-\rho$ relation for the whole range of ice and snow will be one of the important problems on the nature of Greenland ice cap.

§9. Supplementary experiments on the elastic nature of snow and ice at Site 2.

a) *Anisotropy of Peter snow.*

From blocks of Peter snow of one year old, one set of rectangular bars were made so that the width plane coincides with

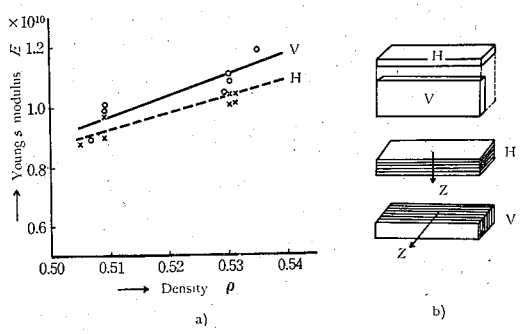

Fig. 26. a) b). Anisotropy of Peter snow; Sample Nos. 23-30, 81-86.

the horizontal plane. This group is marked by H. Another set was made so that the width plane vertical. This is marked by V. If there is any anisotropy in the structure of Peter snow, the YOUNG's modulus is expected to be different for H and V samples. For example, if Peter snow has a horizontal layer structure, it is expected that V samples show a higher value of YOUNG's modulus than H samples, as will be understood from Fig. 26 b). The YOUNG's moduli of H and V samples are shown in Fig. 26 a) as the function of density. The difference is not marked, but it is clear that V is higher than H, showing that Peter snow has a trace of horizontal layer structure.

b) *Age hardening.*

The preliminary experiment on the age hardening was carried out for new soft snow and new Peter snow of 1 day old. Sample Nos. 66 and 67 are new soft snow. After measuring the YOUNG's modulus, these samples were kept in the room at −9°C. The YOUNG's modulus increased to nearly twice of the initial value in one day and then the curve followed the type of saturation curve, as shown in Fig. 27.

The similar experiment was carried out by using Peter snow of 1 day old. The rapid increase of YOUNG's modulns after brought into −9°C room is remarkable. This rapid hardening phenomenon is al-

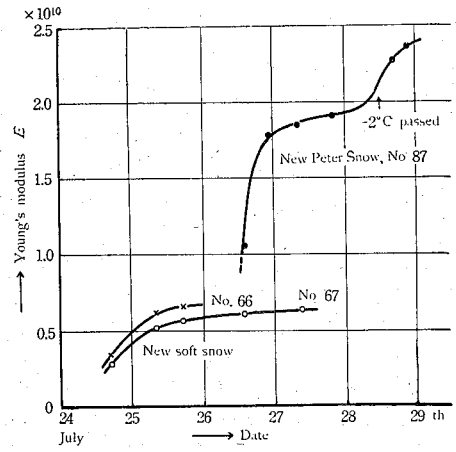

Fig. 27. Age hardening of soft snow and Peter snow.

most completed in half a day or so, and then the curve follows the saturation type. In the morning of 28th the room temperature went up to −2°C for a few hours by accident and then cooled down to −9°C. The YOUNG's modulus made the second jump due to this temperature change, as seen in Fig. 27. The experiments above described are of preliminary nature, but the result shows that this sonic method is very useful in the study of the mechanism of age hardening of snow.

c) *Temperature dependency of YOUNG's modulus of core ice.*

The temperature dependency of YOUNG's modulus was studied with respect to two samples of 1957 core; 26 m depth and 61 m depth. The results are shown in Fig. 28. Although the range of temperature is limited between −2°C and −9°C, the increase in YOUNG's modulus with decrase of temperature is confirmed. The similar experiment was carried out with respect to the tunnel ice; section 11. The temperature dependency is more marked in the case of core samples compared with the case of tunnel ice. This point must be studied further in detail in the future experiment.

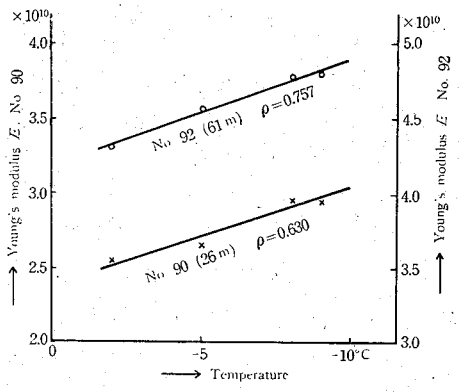

Fig. 28. Temperature dependency of YOUNG's modulus; 1957 core.

§ 10. Viscosity measurement of snow and ice in Greenland.

Viscosity measurement was carried out by the damping method for various samples of snow and ice taken from the ice cap. The damping was fairly rapid at the temperature −5°C or −9°C. Four examples of oscillograms of tunnel ice, new soft snow, coarse grain snow and core sample are shown in Figs. 29–32. The value of $\tan\delta$ was calculated by (13). The loss factor is the largest in the case of new soft snow; Fig. 30, being 0.361, which is the maximum value among all samples tested. The deposited snow of coarse

grains has less value of $\tan\delta$. For the sample of Fig. 31, $\tan\delta$ reduces to 0.0905. When the density increases still further, $\tan\delta$ becomes 0.049 for the core sample of density 0.757; Fig. 32. Fig. 29 shows the mode of damping of the tunnel ice B1, the density of which is 0.908. The value of $\tan\delta$ reduces further to 0.0332. It looks there is a simple relation between density and loss factor, but the frequency dependency is not negligible so that no conclusion can be deduced unless the frequency correction is made. This point will be described in detail in section 12 d).

There is another method of determining $\tan\delta$. Let the resonance frequency be f_{max}. From the resonance curve, the difference of the frequencies Δf is measured, at which the amplitude becomes one half of the maximum amplitude. The meaning of f_{max} and Δf will be understood clearly in Fig. 34. It is known in the viscoelastic theory that

$$\tan\delta = \frac{1}{\sqrt{3}} \frac{\Delta f}{f_{max}} . \qquad (19)$$

The resonance curve is obtained from the oscillogram which is taken by changing the frequency of exciting current successively. One example is shown in Fig. 33. This oscillogram is taken by changing the exciting frequency at 10 cycles interval, starting from $f=250$. The maximum amplitude is observed at $f=310$. The amplitude is measured at each frequency and plotted in Fig. 34. Similar measurement was repeated with respect to the samples of Nos. 49 and 92. It is noticed that the resonance curve shows bilateral symmetry in the case of No. 90, but not in the other cases. The value of $\tan\delta$ for No. 90 calculated from the damping is 0.074, and the value obtained from the resonance curve is 0.071. In this case the agreement is satisfactory.

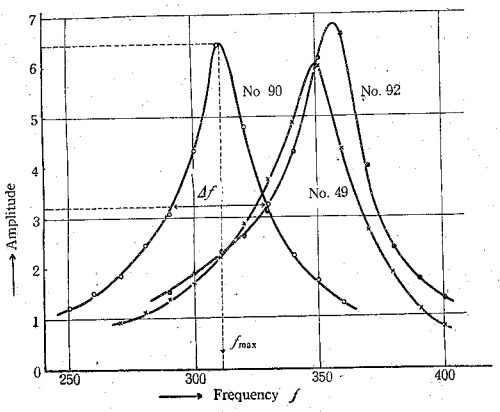

Fig. 34. The resonance curve; amplitude versus frequency.

For the samples of No. 49 and No. 92, the former is 0.0606 and 0.049 respectively, while the corresponding value obtained from resonance curve is 0.078 and 0.064. The difference is much larger than the experimental error. The results of these experiments show that the resonance curve method may be applied when the curve is symmetrical but not when it is unsymmetrical.

The value of $\tan\delta$ obtained for various samples of snow and ice in Greenland was studied in detail, but it was difficult to find some regularities. For example, $\tan\delta$ does not show any simple relation when it is plotted against density. It was found that the frequency dependency plays an important role in this case and no simple relation is obtained as the function of density, when frequency varies for different measurements. The resonance frequency is very sensitive to the size of sample, and it is difficult to carry on the measurement with a fixed value of frequency. In the case of core samples, the frequency varied between 291 and 650, because the sample of enough length could not be obtained for the deep cores.

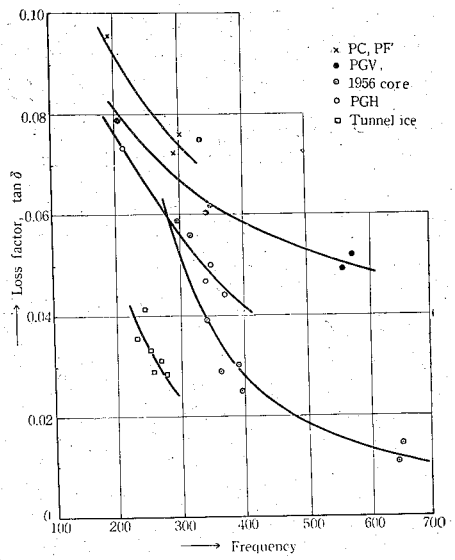

Fig. 35. The frequency dependency of loss factor.

In Fig. 35 the value of $\tan\delta$ is plotted as the function of frequency, irrespective of the density. Each group is expressed as a decreasing function of frequency, and all the curves show more or less similar behavior. This means that the frequency dependency must be taken into account in the case of treating viscous nature of ice or snow.

§ 11. Further experiments on the elastic nature of tunnel ice.

Four samples of tunnel ice cited in Table II of section 4 were brought back to SIPRE laboratory by the aid of dry ice, and

detailed experiments on the visco-elastic nature of these ice samples were carried out in the cold room belonging to this laboratory. The elastic and viscous behaviors were investigated respectively as the function of temperature and frequency.

a) *Temperature dependency of YOUNG's modulus.*

The YOUNG's modulus increases slightly as the temperature decreases and a hysteresis phenomenon is observed. Starting from −5°C, the temperature was lowered to −30°C. The sample was left overnight at −30°C, but not much change was observed in the YOUNG's modulus. The samples were warmed up to −22°C and left overnight. The YOUNG's modulus was almost the same as that observed at −30°C, showing a marked hysteresis phenomenon. When the samples were warmed up to −10°C, the increase in the YOUNG's modulus was about 5% of the former value, except the commercial ice. The nature is similar to the case of hardening of metals by quenching. The results are shown in Fig. 36. This

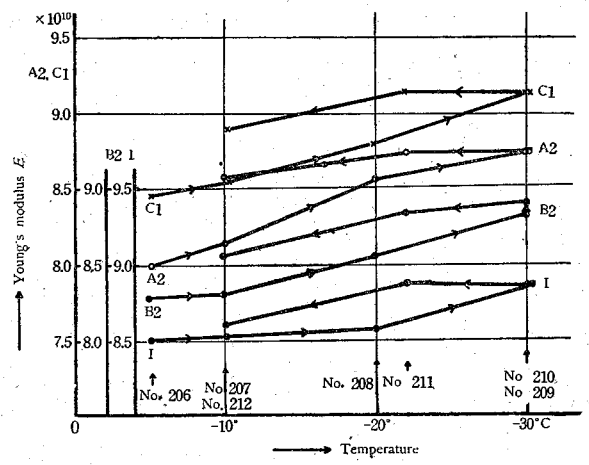

Fig. 36. Hysteresis phenomenon in the relation between YOUNG's modulus and temperature; Nos. 206–212.

hysteresis phenomenon is important for clarifying the elastic nature of this peculiar type of ice.

Taking the mean of the hysteresis curve, the relation between the YOUNG's modulus and temperature is shown in Fig. 37, for four samples of tunnel ice and two samples of commercial ice. Most

of them show the tendency to increase linearly with decrease of temperature, but the rate of increase is a little larger above $-10°C$ than below $-10°C$. Assuming the linear relation

$$\frac{\Delta E}{E} = -\alpha\theta$$

the coefficient α is calculated for the range above $-10°C$. The corresponding values are obtained for core samples, as shown in Fig. 28. Summerizing the results,

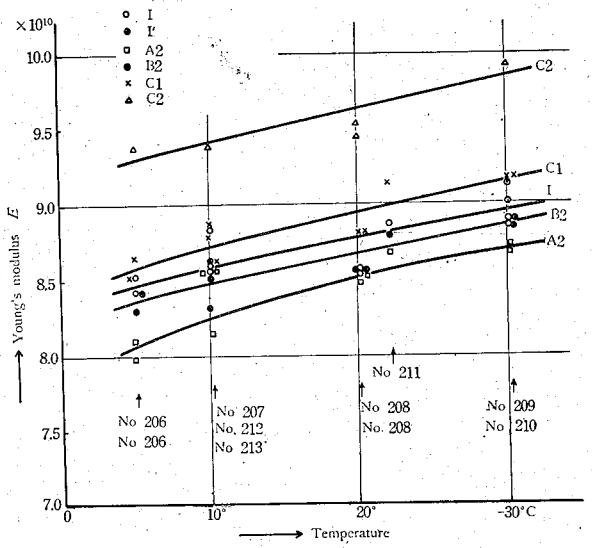

Fig. 37. The relation between YOUNG's modulus and temperature.

$\rho = 0.630$, $\alpha = 0.0281$; 26 m core,
$\rho = 0.757$, $\alpha = 0.0172$; 61 m core,
$\rho = 0.910$, $\alpha = 0.0026$; tunnel ice B, C.

The temperature coefficient decreases with increase in density. In other words, temperature dependency is more marked for compacted snow than ice. For the tunnel ice the coefficient decreases to 0.0021 below $-10°C$.

b) *Frequency dependency of YOUNG's modulus.*

In order to study the effect of frequency on the YOUNG's

modulus, the sample was shortened successively, and the YOUNG's modulus was measured at each stage of shortening of the sample. By this method the YOUNG's modulus can be measured as the function of frequency with respect to one sample. This is an advantage, but there is a disadvantage also; that is, the hysteresis effect if exists cannot be studied by this method.

After finishing the experiments shown in Fig. 36, four samples of I. A2, B2, C1 were made respectively in the same dimension; $l=309.0$ mm, $b=20.0$ mm, $h=6.4$ mm. This size gives the frequency of about 200 cycles. These samples were cut to the length of 185.1 mm, corresponding to the frequency of about 580 cycles, after passing three stages of length. The YOUNG's modulus was measured at each stage and the frequency dependency was obtained; Fig. 38. All samples tested showed the tendency so that

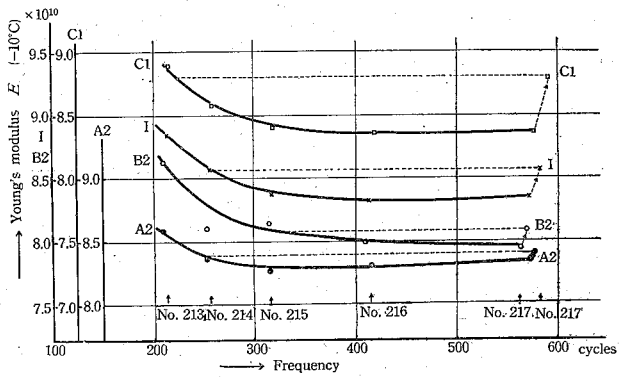

Fig. 38. Frequency dependency of YOUNG's modulus; −10°C, Nos. 213–217′.

the YOUNG's modulus decreases with increase in frequency and tends to approach to a constant value in the higher frequency range. Although the curves are beautiful in form, it cannot be taken to show the frequency dependency of YOUNG's modulus without criticism. After finishing the experiments at the length of 185 mm, No. 217 in Fig. 38, the samples were left overnight at −10°C, and the same measurements were repeated. The value of YOUNG's modulus came back more or less near to the initial value at low frequency, No. 217′ in Fig. 38. This fact shows that some phenomenon like fatigues must be mixed with the effect of

frequency. In fact, in the other series of experiments, sometimes the YOUNG's modulus was found to be constant or nearly constant for the whole range of frequency, 140 cycles through 600 cycles; two series of experiments for A 2 ice in Fig. 39. The data, however, for the commercial ice and C2 ice show the tendency similar to that of Fig. 38. It looks that the ice samples taken from

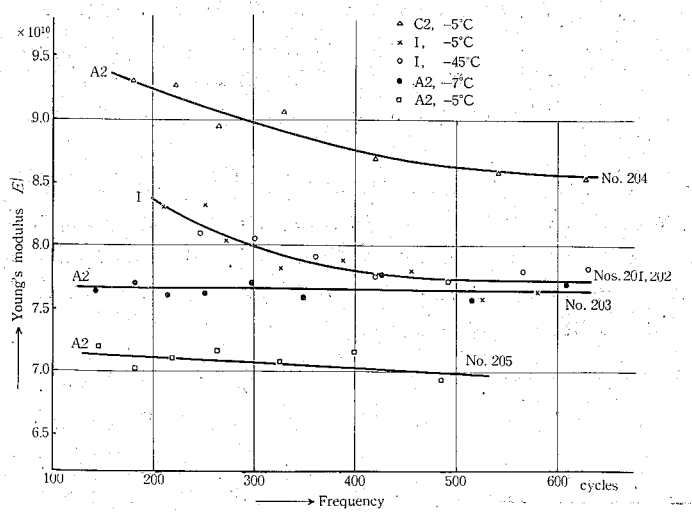

Fig. 39. Frequency dependency of YOUNG's modulus; −4.5°C — −7°C, Nos. 201–205.

Greenland ice cap have such a variety in their elastic nature that any hasty conclusion will not be desirable. In any case the effect of frequency is not so intensive in the case of YOUNG's modulus, and the frequency effect may be neglected if 10% error is admitted in the discussion of the results. The frequency dependency, however, is a powerful tool for the physical investigation of the visco-elastic properties of ice, and further investigations are desirable to be carried out in this line.

§ 12. Further experiments on the viscous nature of tunnel ice.

a) *The oscillograms.*

In order to give the general idea of the mode of damping, the oscillograms of different samples under various conditions are

illustrated in Figs. 40–47. The effect of temperature is most conspicuous in the case of the sample of C2 ice. The mode of damping of C2 ice at various temperatures is shown in Fig. 40–43. Fig. 40 shows the damping of C1 ice at −5°C, instead of C2 ice, because no datum is available for C2 ice at −5°C. The difference is negligible between C1 and C2 at this temperature, although it is sensible at the temperatures below −20°C. As seen in the oscillograms, the rate of damping decreases remarkably as the temperature becomes lower. The loss factor at −30°C is only 1/35 of that at −5°C. This means that the activation energy is fairly large for C2 ice.

The comparison is made among the commercial ice I, A2, B2 and C1 at −20°C. The oscillograms are shown in Figs. 44–47. It is confirmed from these pictures that the loss factor of the samples taken from ice cap, B2 and C1, is much smaller than that of commercial ice or superimposed ice.

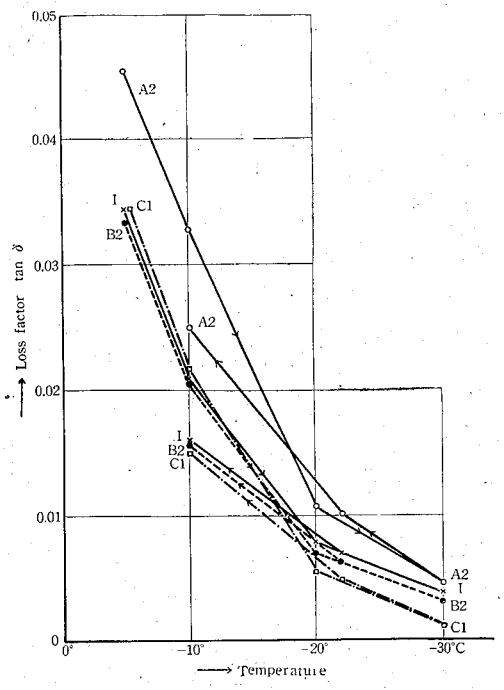

Fig. 48. Hysteresis phenomenon in the relation between loss factor and temperature.

b) *Temperature dependency of loss factor.*

The temperature dependency was studied in the range of −5°C and −30°C. The similar hysteresis phenomenon as the case of YOUNG's modulus was observed in the viscous nature of ice. When the sample was cooled down to −30°C, the loss factor decreased remarkably, showing that the energy loss due to internal friction diminishes rapidly with decrease in temperature. Then the sample was warmed up to −10°C. In that case tanδ showed a smaller value than the former value at −10°C.

The results are shown in Fig. 48. As $\tan\delta$ is a measure of non-elastic nature of the material, this hysteresis behavior corresponds to the increase in YOUNG's modulus by the same process, as described in Fig. 36.

In order to correlate the loss factor to the internal viscosity, it is necessary to adopt some model. As the first approximation, the well known two simple models will be considered; that is, VOIGT model and MAXWELL model. According to (14), the coefficient of viscosity is proportional to $\tan\delta$ for VOIGT model, and inversely proportional in the case of MAXWELL model. In order to compromise with the conception of the ordinary viscosity, η must increase with decrease in temperature. In this meaning MAXWELL model is adopted in this case. YOSIDA[16] also took up MAXWELL model in his study of deposited snow for the same reason, and succeeded to develop his theory of mechanics of snow. Adopting MAXWELL model, the viscosity coefficient η is calculated by

$$\eta = \frac{E}{\omega \tan\delta} . \qquad (20)$$

Putting aside the hysteresis portion of the curves in Fig. 48, η is calculated by (20), and is plotted against temperature; Fig. 49. All curves show an exponential form, which is familiar in the case of viscosity of ordinary liquid expressed as the function of temperature. MAXWELL model, therefore, is considered to be a good choice in this case.

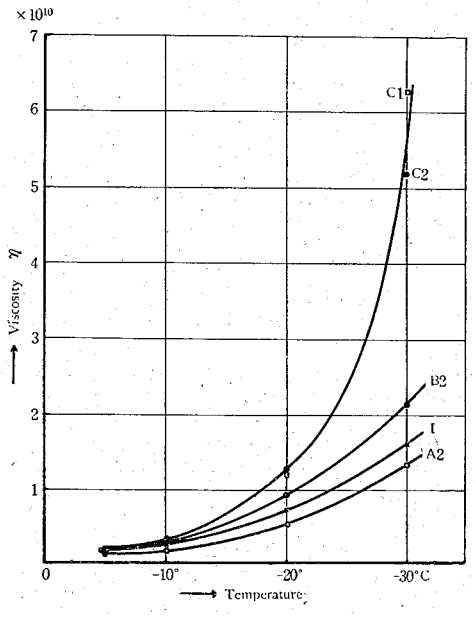

Fig. 49. Temperature dependency of viscosity; MAXWELL model, Nos. 206–212.

c) *The activation energy.*

The logarithm of viscosity calculated by using MAXWELL model was plotted against the reciprocal of absolute temperature, and it was found that a linear relationship held for each of the samples;

Fig 50. The datum of C1 ice at −5°C is the only exception, which is excluded in this discussion. The relation is expressed by

$$\eta = \text{Const. } \exp\left(+\frac{F}{RT}\right), \qquad (21)$$

in which F is the activation energy, R the gas constant, T the absolute temperature. From the slope of the line, the activation energy is calculated as follows.

F=12.7 Kcal/mol
for commercial ice,
F=13.5Kcal/mol
for superimposed ice A2,
F=13.9 Kcal/mol
for the ice with elongated bubbles B2,
F=18.7 Kcal/mol
for the ice with small bubbles C1 and C2.

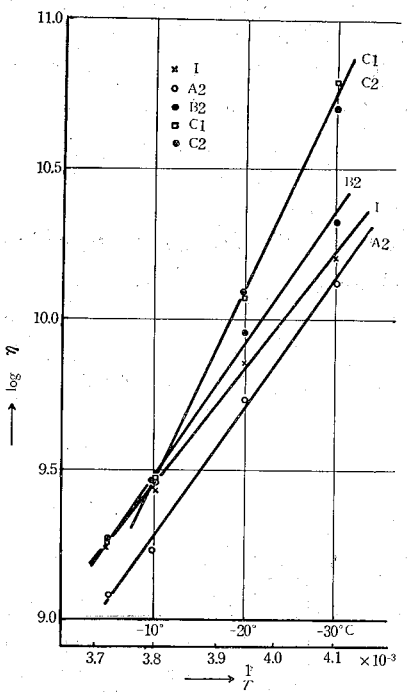

Fig. 50. Calculation of the activation energy.

The activation energy of C1 and C2 ices is considerably large. This ice is taken at the spot 680 feet from the entrance of the ice tunnel, and is considered to be very old and have been kept under an intensive stress for very long time. Judging from the size and shape of air bubbles, B2 ice must be much less old than C ice. The superimposed ice A2 is of course very new compared with the two ices mentioned above. It is an interesting phenomenon that the activation energy is larger for the older ice, although the density is almost the same for all these samples.

We adopted MAXWELL model in this calculation, but the value of activation energy does not change if VOIGT model is employed. In that case the equation becomes

$$\eta = \text{Const. } \exp\left(-\frac{F}{RT}\right)$$

and the value of F remains the same.

d) *Frequency dependency of loss factor and viscosity.*

The loss factor is plotted against frequency in Fig. 51. The experiments at −10°C were carried out more carefully than the other case. In the case of ice cap samples B 2 and C 1, the loss factor decreases sensibly with increase in frequency within the range of 200 and 350 cycles, but above 350 cycles it is almost independent of frequency. The commercial ice also follows the same course. The superimposed ice A 2, however, behaves in a little different way, the frequency dependency being more marked.

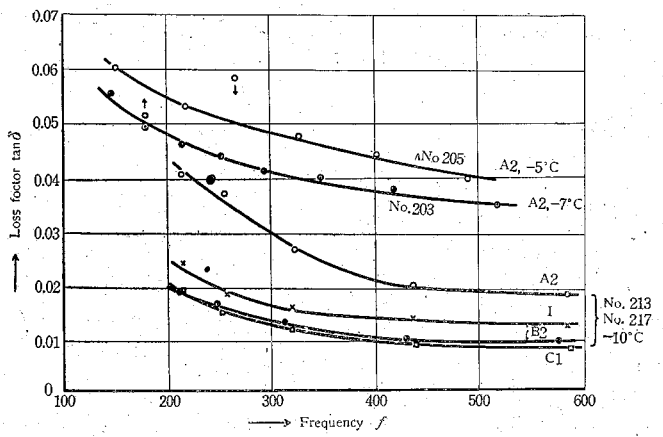

Fig. 51. Frequency dependency of tan δ; Nos. 203, 205, 213–217.

Adopting MAXWELL model, Fig. 51 is transformed into Fig. 52, which shows the frequency dependency of viscosity. It is very interesting that the viscosity is almost constant in the wide range of frequency between 200 and 500 cycles in the case of experiments carried out at −10°C, when MAXWELL model is used. The frequency was extended to 100 cycles in the other experiments, and gradual decrease in viscosity was observed with increase in frequency within the range of smaller frequencies. This curve will be used later for making the frequency correction of viscosity in the viscosity-density diagram; Fig. 54. The points marked with arrows in Fig. 51, which deviate considerably from the tan $\delta - f$ curve, are now found on the $\eta - f$ curve in Fig. 52. This is due to the deviation in the value of E, which compensates the deviation in tan δ; see eq (20).

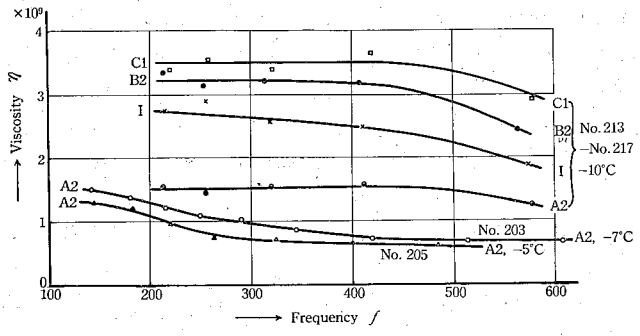

Fig. 52. Frequency dependency of viscosity; MAXWELL model, Nos. 203, 205, 213–217.

§ 13. Relation between viscosity and density.

The loss factor is a function of density and frequency. The series of curves in Fig. 35 is drawn irrespective of density, and shows the superimposed effect of frequency and density. In Fig. 51 the frequency dependency is shown for each of the samples, the density being constant for each of the curves in this case. Referring to the ice cap samples B2 and C1, $\tan\delta$ is constant within the error of $\pm 20\%$ when the data above 250 cycles are chosen. In order to get the rough idea of the relation between loss factor and density, the data above 250 cycles were picked up

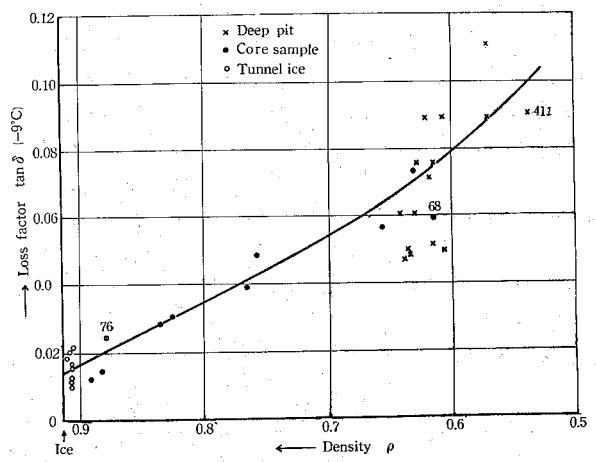

Fig. 53. The relation between loss factor and density.

and Fig. 53 was constructed. As the frequency correction is not made, the points are scattered in a wide range, but the tendency of the curve is well recognized. From ice to the sample of density about 0.6, the loss factor increases linearly with decrease in density, and the rate of increase becomes larger below density 0.6.

The variation of viscous nature as the function of density is more clearly seen when the viscosity coefficient of MAXWELL model is plotted against density, because the viscosity is constant in the wide range of frequency as shown in Fig. 52. All available data are plotted irrespective of frequency in Fig. 54, in which the logarithm of viscosity is taken as ordinate. The relation is expressed by the full line. No frequency correction is necessary in the range of density above 0.58, the point marked by 41 in Fig. 54, because the frequency used is above 250 cycles.

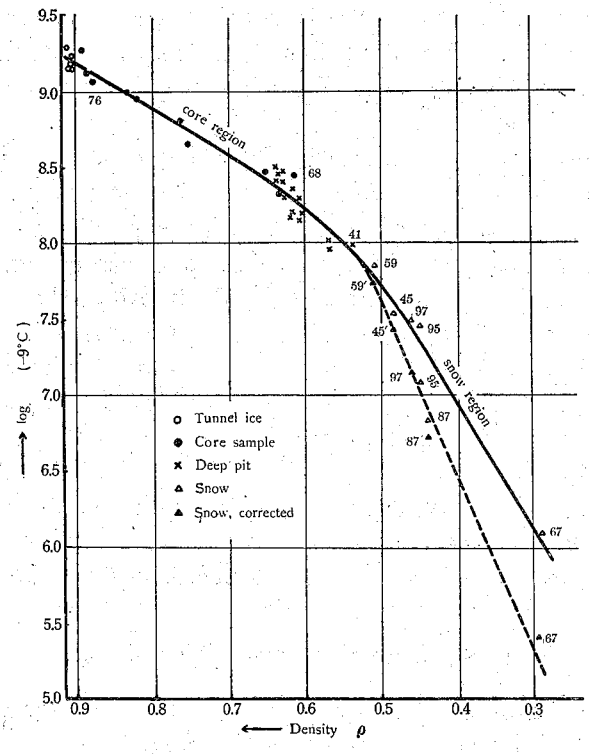

Fig. 54. The relation between viscosity and density; −9°C, frequency between 200–400 cycles.

In the range of density below about 0.5; that is, in the range of soft snow, the frequency between 105 and 222 cycles was used. No data is available as for the frequency dependency of snow samples in this frequency range, but the correction is made tentatively by assuming that the frequency dependency is similar to the curves No. 203 and No. 205 in Fig. 52, and the value of η corresponding to the frequency between 200 and 400 cycles is calculated, within which range η is assumed to be independent of frequency in the case of snow samples also. The uncorrected data for snow samples are shown by white triangles in Fig. 54, and the corrected values by dark triangles. If this correction is adequate, the $\log\eta-\rho$ relation will follow the broken line in Fig. 54 within the range of lower densities than 0.538; that is, in the range of soft snow. Whether this correction is adequate or not, it will be an established fact that $\log\eta$ decreases almost linearly with decrease in density until it reaches about 0.55 and the rate increases for the lower densities. In the snow region; that is, below 0.5 of density, another linear relationship is observed with the steeper slope.

Comparing this result with $E-\rho$ relation in Fig. 25, it is noticed that the YOUNG's modulus and viscosity show the similar behavior as the function of density. The region below the density 0.9 is divided into two regions; the core region and the snow region. For both YOUNG's modulus and viscosity, the relation with respect to density is different for these two regions. In the case of viscosity the core region is between the densities of 0.9 and 0.55, whereas it is between 0.9 and 0.50 for YOUNG's modulus. The transition of one region to the other cannot be abrupt but must be gradual. The lower limit of the core region may be 0.50 or 0.55. The difference is not essential. The difference between the ice region and the core region is not clearly seen in the value of viscosity, although it is marked in the case of YOUNG's modulus.

§ 14. Summery and discussion.

The measurement of YOUNG's modulus and loss factor was carried out by the sonic method with respect to ice and snow in Greenland ice cap. The sample is cut in the shape of a rectangular

bar, and the resonance frequency of its lateral vibration was measured for the calculation of YOUNG's modulus. The loss factor was measured by the damping method. In case of metals, the torsional vibration is usually used for the same purpose, but this method is difficult to be applied for ice or snow, because the sample cannot be made so thin due to the quick evaporation of ice. Besides, the clamping of the sample is very difficult in the case of snow or ice.

Three kinds of ice and snow samples were used. The first is the ice samples taken from the wall of ice tunnel at Tuto, which is dug into the edge of ice cap. The sample is almost ice containing a small air void, the density being near to that of pure ice. This kind is called the tunnel ice in this report. The second is the samples taken from the wall of the deep pit of 100 feet depth, which is dug at Site 2, and the core samples obtained by drilling in the ice cap. This type is the intermediate state of snow and ice, and is called the core samples. The third is the snow near the surface of ice cap.

YOUNG's modulus density relation was obtained for the whole range of snow and ice observable in Greenland ice cap. The result shows that the whole region is divided into three regions. The tunnel ice belongs to Region I, the density being between 0.917 and 0.90. In Region I YOUNG's modulus decreases very rapidly when the density deviates slightly from that of pure ice. Region II covers the range of density between 0.90 and 0.50. The core samples belong to this region. The relation between YOUNG's modulus and density is expressed by a straight line for the whole range of this region. The empirical formula of this line is

$$E = (16.4\rho - 7.20) \times 10^{10} .$$

Snow samples near the surface of ice cap belong to Region III. The YOUNG's modulus decreases in an exponential form as the density decreases in this region. The empirical formula takes the form

$$E = C \exp\left\{-k(0.50-\rho)\right\} .$$

k is a factor determined by the structure of snow, and is called "structure factor". For the ordinary settled snow k is 6.35 and

the empirical formula is

$$\log E = 6.80 + 6.35\,\rho\,.$$

The structure factor of wind packed snow is smaller than that of ordinary settled snow, and for the granular snow the reverse is the case. If the structure of snow is examined by making thin sections and is correlated to k, this structure factor will be introduced effectively into the mechanics of snow. The physical interpretation of this $E-\rho$ relation for the whole range of ice and snow will be one of the important problems in the future.

Both the YOUNG's modulus and the loss factor are the function of temperature and frequency. Bringing back some samples of tunnel ice to SIPRE laboratory, the temperature dependency and the frequency dependency were examined. The YOUNG's modulus showed a slight increase as the temperature is lowered. The loss factor decreased very rapidly when the temperature became lower. Adopting MAXWELL model the loss factor $\tan\delta$ was converted into the coefficient of viscosity η by the following equation

$$\eta = \frac{E}{\omega \tan\delta}\,,$$

in which ω is the angular frequency. η increases in an exponential form with decrease in temperature, and $\log\eta$ is expressed by a straight line when plotted as the function of $1/T$, T being the absolute temperature.

$$\eta = \text{Const. } \exp\left(+\frac{F}{RT}\right).$$

F is the activation energy, R the gas constant. From the slope of the line, the activation energy is calculated as follows.

$F=12.7$ Kcal/mol for commercial ice,
$F=13.5$ Kcal/mol for superimposed ice taken at Tuto,
$F=13.9$ Kcal/mol for the tunnel ice with elongated bubbles,
$F=18.7$ Kcal/mol for the ice taken at 680 feet from the entrance of ice tunnel.

The frequency dependency of YOUNG's modulus is complicated, but not so large. In the case of loss factor, the effect is considerable, and no simple relation is observed between $\tan\delta$ and ρ, when

the data are plotted irrespective of the frequency used. However, the frequency dependency becomes very small when viscosity η is used instead of loss factor. A simple relation, therefore, is obtained when η is plotted against density. It was found that $\log \eta$ decreases almost linearly with decrease in density until it reaches about 0.55 and the rate increases for the lower densities. In the snow region; that is, below 0.5 of density, another linear relationship is observed with the steeper slope. Comparing this result with $E-\rho$ relation, it is noticed that the YOUNG's modulus and viscosity show the similar behavior as the function of density. From these results it was concluded that the visco-elastic meter by using the sonic method is a powerful tool for the study of elastic and viscous nature of snow and ice in Greenland ice cap.

Literatures

1) DE QUERVAIN, M. (1946): Kristallplastische Vorgänge im Schneeaggregat II. Mitteilungen aus dem eidg. Institute für Schnee- und Lawinenforschung.
2) GLEN, J. W. (1952): Experiments on the deformation of ice. Journal of Glaciology, Vol. 2, pp. 111–114.
3) GLEN, J. W. & PERUTZ, M. F. (1954): The growth and deformation of ice crystals. Journal of Glaciology, Vol. 2, pp. 397–403.
4) STEINEMANN, SAMUEL (1954): Results of preliminary experiments on the plasticity of ice crystals. Journal of Glaciology, Vol. 2, pp. 404–412.
5) GRIGGS, D. T. & COLES, N. E. (1954): Creep of single crystals of ice. SIPRE Report 11.
6) LANDAUER, J. K. (1955): Stress-strain relation in snow under uniaxial compression. Journal of Applied Physics, Vol. 26, pp. 1493–1497.
7) JELLINEK, H. H. G. & BRILL, R. (1956): Viscoelastic properties of ice. Journal of Applied Physics, Vol. 27, pp. 1198–1209.
8) YAMAJI, K. & KUROIWA, D. (1954): Study of elastic and viscous properties of snow by the vibration method, I. Teion Kagaku, A, Vol. 13, pp. 49–57, (In Japanese).
9) KUROIWA, D. & YAMAJI, K. (1956): Study of elastic and viscous properties of snow by the vibration method, II. Teion Kagaku, A, Vol. 15, pp. 43–57, (In Japanese).
10) LORD RAYLEIGH. (1925): Theory of Sound, Vol. I, pp. 273–278, London.
11) STAVERMAN, A. J. and SCHWARZI, F. (1956): Linear deformation behavior of high polymers. Die Physik der Hochpolymeren, Bd. IV, pp. 23–33, Springer-Verrag, Berlin.
12) YOSIDA, Z. and collegues (1956): Physical studies of deposited snow, II. Con-

tributions from the Institute of Low Temperature Science, Hokkaido University, No. 9, pp. 37–40.

13) NAKAYA, U. (1956): Properties of single crystals of ice, revealed by internal melting. SIPRE Report 13.

14) LANGWAY, C. C. Jr. Will appear shortly in SIPRE Report.

15) FUCHS, A. (1956): Preparation of plastic replicas and thin sections of snow. SIPRE Technical Report, No. 41.

16) YOSIDA, Z. and collegues, loc. cit.

APPENDIX

The data of experiments, in which both Young's modulus and loss factor are measured, are cited in this Table.

No.	Ice	ρ	f	tan δ	$E\times10^{10}$	$\eta\times10^{8}$	log η	Notes
T 2	B 1	0.908	254	0.0332	8.3	15.7	9.196	−50°C. MP2H elongated bubbles. Fig. 29
T 5	E 1	0.910	233	0.0354	7.5	14.5	9.161	−4.8°C. MP4H many small bubbles.
T 6	B 1	0.906	268	0.0284	8.1	17.0	9.230	−4.8°C. MP2V elongated bubbles.
T 7	E 1	0.910	263	0.0312	8.0	15.5	9.190	−4.8°C. MP4H many small bubbles.
T 9	E 2	0.913	265	0.0287	9.1	19.2	9.283	−4.2°C. MP4V many small bubbles.
T11	B 1	0.908	243	0.0416	7.8	12.3	9.089	MP2, elongated (z).
39	D 2	0.570	291	0.111	1.86	0.917	7.962	Deep pit. Coarse grain.
40	D 3	0.569	286	0.136	1.79	0.741	7.870	Coarse grain.
41	E 2	0.538	281	0.0906	1.53	0.959	7.982	Coarse grain. Fig. 13.
42	E 3	0.570	309	0.0886	1.78	1.035	8.015	Coarse grain.
43	F 2	0.620	337	0.089	2.77	1.465	8.164	
44	F 3	0.605	337	0.089	2.64	1.395	8.144	
45	B 3	0.487	191	0.175	0.76	0.361	7.557	
46	G H	0.635	350	0.050	3.21	2.92	8.464	Deep pit G. Fig. 12.
47	G V	0.630	352	0.062	3.28	2.395	8.380	Comparison of H and V the effect of size Fig. 13.
48	G H	0.640	368	0.044	3.19	3.14	8.497	
49	G V	0.640	348	0.0606	3.28	2.47	8.392	
50	G H	0.642	214	0.073	3.10	3.16	8.500	
51	G V	0.612	210	0.079	2.91	2.87	8.444	
52	G H	0.634	340	0.047	2.96	2.96	8.471	
53	G V	0.628	339	0.076	3.19	1.98	8.296	
54	G V	0.602	560	0.049	2.67	1.55	8.190	
55	G V	0.615	575	0.052	2.74	1.455	8.162	

No.	Ice	ρ	f	tan δ	$E\times10^{10}$	$\eta\times10^{8}$	log η	Notes
56	F′	0.616	294	0.072	2.91	2.19	8.340	Deep pit, 2 years old.
58	F′	0.613	306	0.076	2.82	1.93	8.286	
59	C′	0.504	197	0.096	0.83	0.705	7.848	
67		0.288	105	0.361	0.028	0.0117	6.068	Soft snow. Start of age hardening, Fig. 30.
68		0.612	302	0.0588	3.05	2.74	8.438	21 m 1956 core. Fig. 16.
70		0.656	319	0.0559	3.30	2.95	8.470	24.5 m
72		0.763	340	0.0392	5.91	6.19	8.792	50.5 m
74		0.833	361	0.0286	6.40	9.84	8.993	80.5 m
75		0.823	386	0.0302	6.72	9.20	8.964	80.5 m
76		0.878	395	0.0254	7.20	11.4	9.057	122 m
78		0.895	640	0.0113	7.52	16.5	9.217	155 m
79		0.884	650	0.0142	7.53	13.0	9.114	155 m
87		0.440	222	0.191	0.184	0.069	6.838	Peter snow (26th 1430) Age hardening of new.
90		0.630	308	0.074	2.96	2.07	8.316	26 m 1957 core.
92		0.757	360	0.049	4.78	4.31	8.634	61 m. Fig. 32.
95		0.450	121	0.116	0.308	0.359	7.544	Settled granular snow. 0.5 m from wall.
97		0.466	130	0.143	0.426	0.366	7.563	Less granular 2 m from wall. Fig. 23.

SIPRE Lab.

No.	Ice	ρ	f	tan δ	$E\times10^{10}$	$\eta\times18^{8}$	log η	Notes
203	A 2	0.915	142	0.056	7.64	15.3	9	Tunnel Ice. −7°C. superimposed ice.
		0.915	180	0.0493	7.70	13.8	9	Few tiny bubbles.
		0.915	213	0.047	7.60	12.2	9	
		0.915	249	0.045	7.60	10.8	9	
		0.915	394	0.041	7.70	10.1	9	
		0.915	345	0.0405	7.58	8.63	8	

No.	Ice	ρ	f	tan δ	$E \times 10^{10}$	$\eta \times 10^{8}$	log η	Notes
203	A 2	0.915	420	0.0392	7.78	7.50	8	
		0.915	515	0.034	7.56	6.87	8	
		0.915	610	0.0308	7.72	6.52	8	
204	C 2	0.911	177	0.0332	9.30	25.2		Tunnel Ice. −50°C. many tiny bubbles.
205	A 2	0.915	147	0.060	7.20	12.9		Tunnel Ice. −5°C. superimposed ice.
		0.915	180	0.051	7.02	12.2		
		0.915	217	0.054	7.10	9.65		
		0.915	263	0.059	7.16	7.36		
		0.915	325	0.0477	7.07	7.24		
		0.915	400	0.0439	7.45	6.74		
		0.915	485	0.0394	7.21	6.01		
206	I	0.917	239	0.0344	8.50	16.5	9.217	−5°C. Temperature dependency.
	A 2	0.915	230	0.0455	7.98	12.2	9.085	
	B 2	0.910	209	0.0333	8.30	18.9	9.277	
	C 2	0.911	211	0.0345	8.47	18.4	9.264	
207	I	0.915	240	0.0209	8.54	27.0	9.431	−10°C. Temperature dependency.
	A 2	0.910	232	0.0327	8.13	17.0	9.230	
	B 2	0.910	210	0.0207	8.31	30.4	9.482	
	C 1	0.911	212	0.0217	8.54	29.5	9.470	
	C 2	0.910	250	0.0206	9.39	29.0	9.462	
208	I	0.817	241	0.00793	8.58	71.5	9.854	−20°C. Temperature dependency.
	A 2	0.915	238	0.01060	8.55	54.0	9.732	
	B 2	0.910	212	0.00691	8.55	93.0	9.968	
	C 1	0.911	215	0.00543	8.79	119.8	10.078	
	C 2	0.910	252	0.00492	9.52	122.5	10.088	

No.	Ice	ρ	f	tan δ	$E\times10^{10}$	$\eta\times10^{8}$	log η	Notes
209	I	0.917	245	0.00366	8.89	158.0	10.199	−30°C. Temperature dependency.
	A 2	0.915	240	0.00439	8.73	131.6	10.120	
	B 2	0.910	216	0.00309	8.85	211.0	10.324	
	C 1	0.911	219	0.00106	9.14	628.0	10.798	
	C 2	0.910	257	0.00120	9.91	512.0	10.708	
210	I 1	0.917	245	0.00410	8.89	140.5	10.148	Repeat No. 209, over-night at −30°C.
	A 2	0.915	240	0.00452	8.73	128.5	10.108	
	B 2	0.910	217	0.00302	8.92	216.0	10.334	
211	I	0.917	245	0.00693	8.89	83.0	9.918	−22°C. Temperature dependency
	A 2	0.915	240	0.00997	8.73	58.2	9.764	Warm up from −30°C.
	B 2	0.910	216	0.00603	8.85	108.2	10.034	
	C 1	0.911	219	0.00478	9.15	139.0	10.142	
212	I	0.917	241	0.016	8.60	35.4	9.547	−10°C. Temperature dependency
	A 2	0.915	238	0.0250	8.57	22.9	9.359	warm up from −22°C over-night at −10°C.
	B 2	0.910	212	0.0156	8.55	41.0	9.612	
	C 1	0.911	216	0.0153	8.88	42.6	9.628	
213	I 1	0.917	215	0.0242	8.85	27.1	9	Repeat No. 212 all 6.4 mm −10°C, over-night.
	A 2	0.915	212	0.0407	8.58	15.85	9	Start of frequency dependency.
	B 2	0.910	213	0.0193	8.62	33.3	9	
	C 1	0.911	216	0.0196	8.88	33.2	9	
214	I	0.917	258	0.0185	8.55	28.5	9	Frequency dependency at −10°C.
	A 2	0.915	255	0.0370	8.35	14.05	9	
	B 2	0.910	255	0.0167	8.08	30.6	9	
	C 1	0.911	252	0.0152	8.56	55.1	9	
214	I	0.917	258	0.0185	8.55	28.5	9	Frequency dependency at −10°C.
	A 2	0.915	255	0.0370	8.35	14.05	9	

No.	Ice	ρ	f	tan δ	$E\times10^{10}$	$\eta\times10^{8}$	log η	Notes
214	B 1	0.910	252	0.0167	8.08	30.6	9	
	C 1	0.911	259	0.0152	8.56	35.1	9	
215	I	0.917	322	0.0167	8.36	24.8	9	Frequency dependency at −10°C.
	A 2	0.915	321	0.0274	8.25	14.9	9	
	B 2	0.910	319	0.0129	8.14	31.5	9	
	C 1	0.911	324	0.0124	8.39	33.1	9	
217	I	0.917	575	0.0130	8.31	17.7	9	Frequency dependency at −10°C.
	A 2	0.915	578	0.0192	8.31	11.9	9	
	B 2	0.910	565	0.0095	7.91	23.5	9	
	C 1	0.911	580	0.0081	8.34	28.4	9	
217′	I	0.917	585	0.0166	8.53	14.0	9	Repeat No. 217 over-night at −10°C.
	A 2	0.915	580	0.0252	8.37	9.1	8	
	B 2	0.910	570	0.0136	8.05	16.6	9	
	C 1	0.911	595	0.0128	8.79	18.4	9	

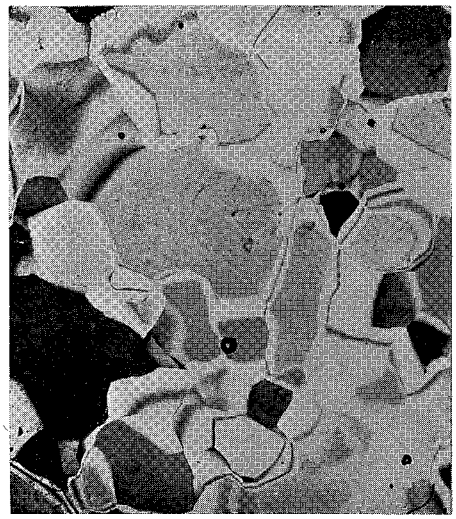

Fig. 3. A 2 ice, superimosed ice, $\rho = 0.915$, $\times 7.5$.

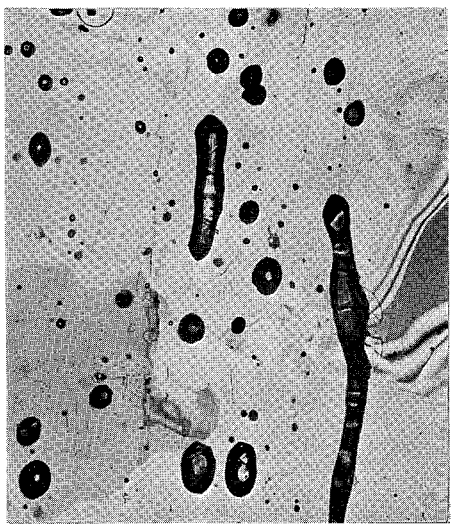

Fig. 4. B 2 ice, ice cap ice, $\rho = 0.910$, $\times 7.7$.

Fig. 5. C 1 ice, 680′ from the entrance of the tunnel; $\rho = 0.911$, $\times 7.5$.

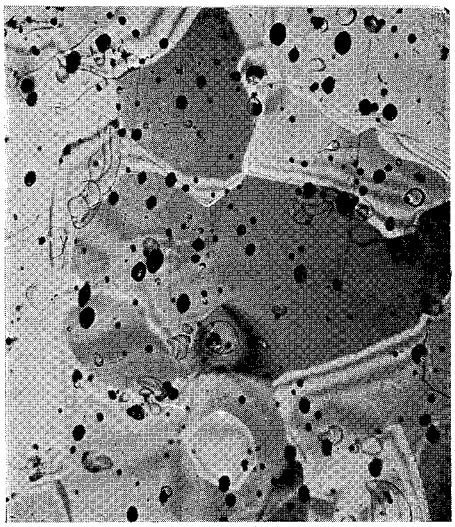

Fig. 6. C 2 ice, 680′ from the entrance of the tunnel; $\rho = 0.910$, $\times 7.5$.

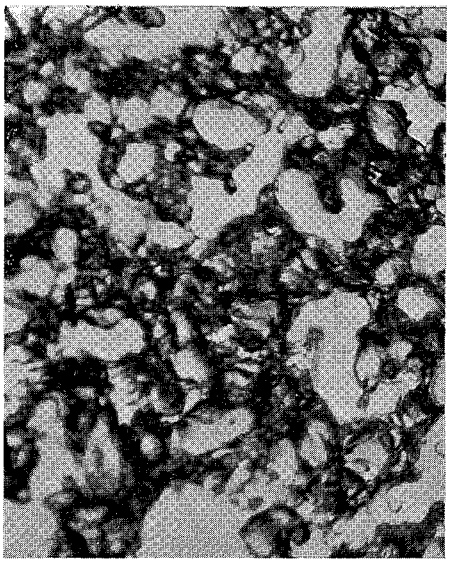

Fig. 8. Deep pit PB, $\rho = 0.49$, × 10.5.

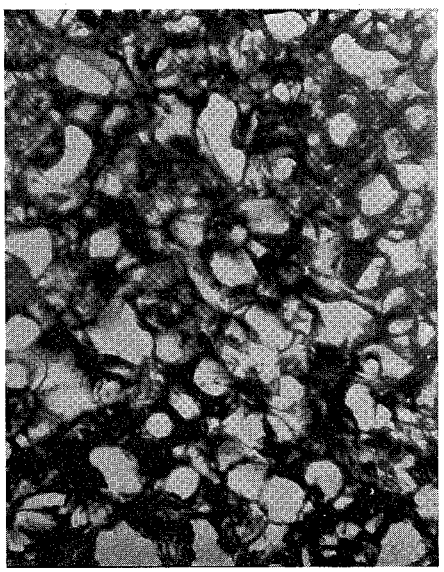

Fig. 9. Deep pit PD, $\rho = 0.57$. × 10.5.

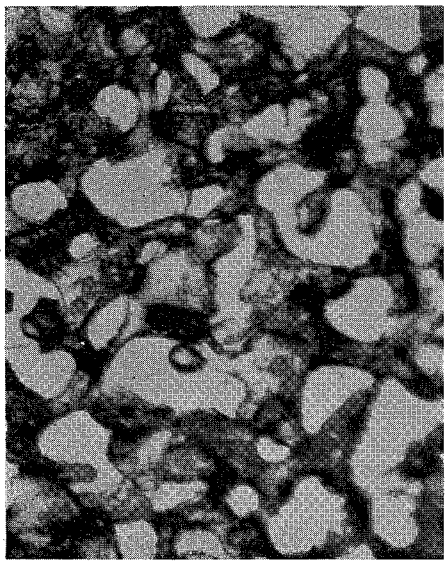

Fig. 10. Deep pit PF, $\rho = 0.61$, × 10.5.

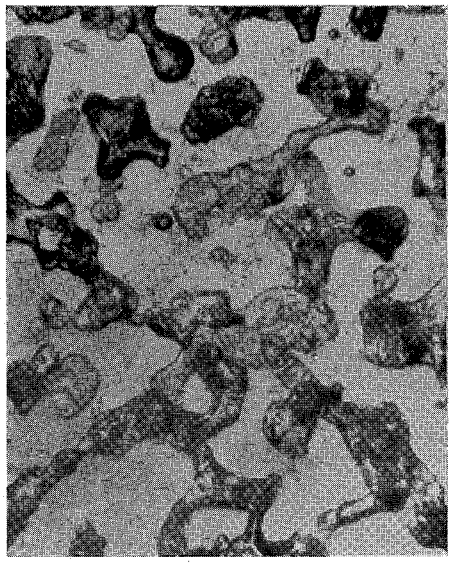

Fig. 11. Deep pit PG, $\rho = 0.64$, × 10.5.

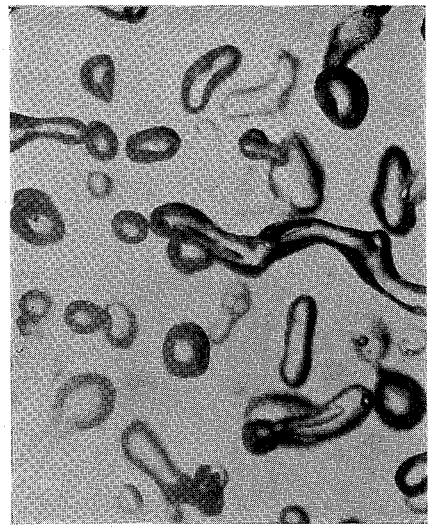

Fig. 14. 1956 core, 84 m,
$\rho = 0.880$, $\times 10.5$.

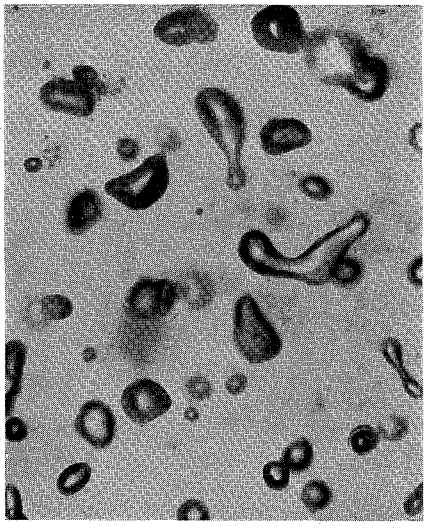

Fig. 15. 1956 core, 113 m,
$\rho = 0.899$, $\times 10.5$.

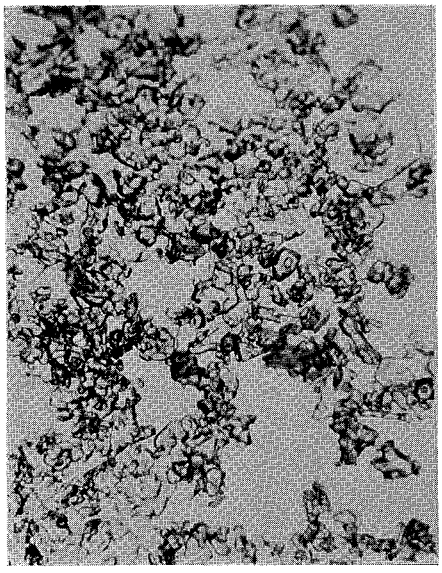

Fig. 20. Wind packed snow,
$\rho = 0.35$, $\times 10.5$.

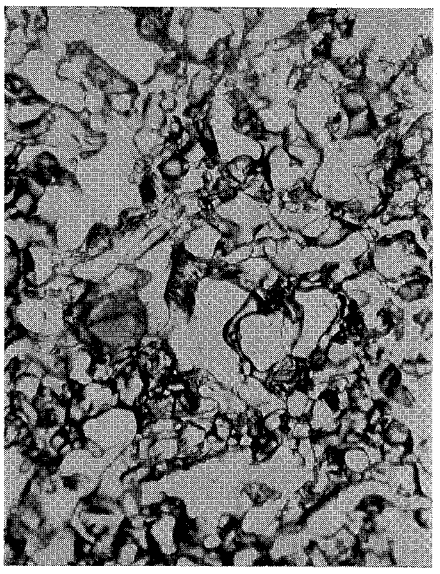

Fig. 21. Peter snow, one year old,
$\rho = 0.53$, $\times 10.5$.

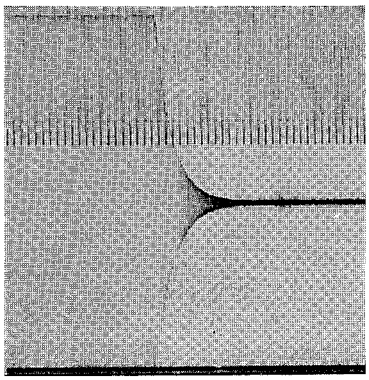

Fig. 29. Tunnel ice No T 2, $\rho=0.908$, $f=254$, $E=8.3\times10^{10}$, $\tan\delta=0.0332$, -5°C.

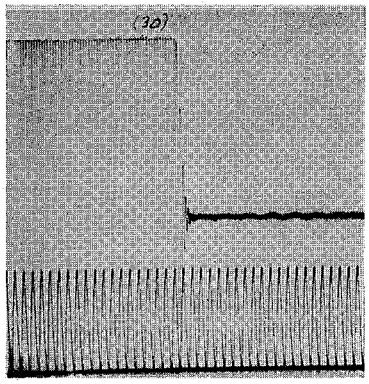

Fig. 30. New soft snow, No. 67, $\rho=0.288$, $f=105$, $E=0.028\times10^{10}$, $\tan\delta=0.361$, -9°C.

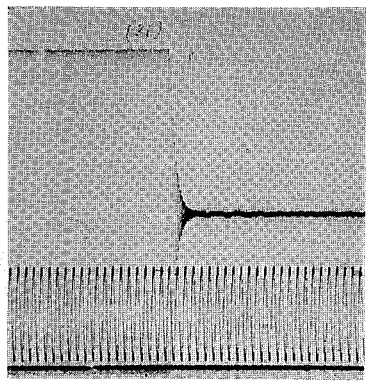

Fig. 31. Coarse grain snow, No. 41. $\rho=0.538$, $f=281$, $E=1.53\times10^{10}$, $\tan\delta=0.0905$, -9°C.

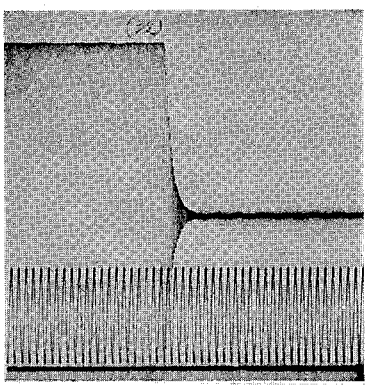

Fig. 32. 1957 core, No. 92, 61 m, $\rho=0.757$, $f=360$, $E=4.78\times10^{10}$, $\tan\delta=0.049$, -9°C.

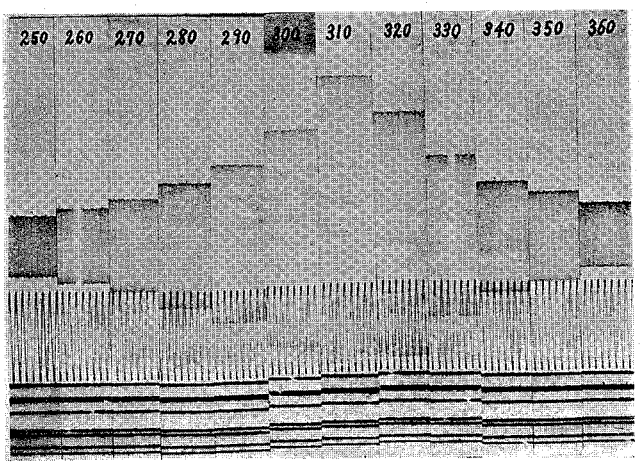

Fig. 33. 1957 core, 26 m; No. 90, $\rho=0.630$, $E=2.96\times10^{10}$, $\tan\delta=0.074$.

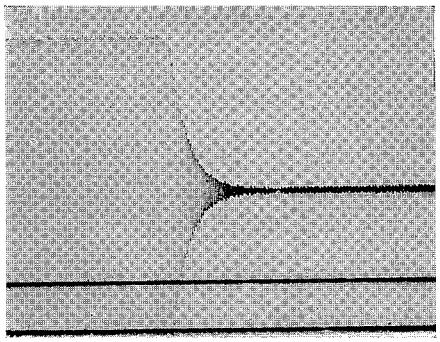

Fig. 40. C 1 ice, No. 206, −5°C, $\rho=0.911$, $E=8.47\times10^{10}$, $\tan\delta=0.0345$.

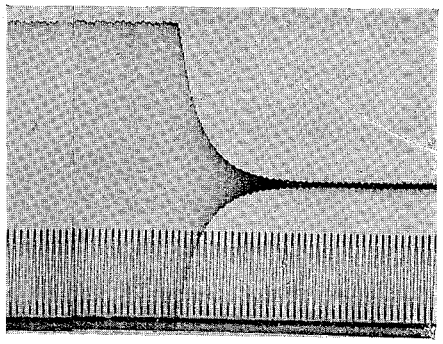

Fig. 41. C 2 ice, No. 207, −10°C, $\rho=0.910$, $E=9.39\times10^{10}$, $\tan\delta=0.0206$.

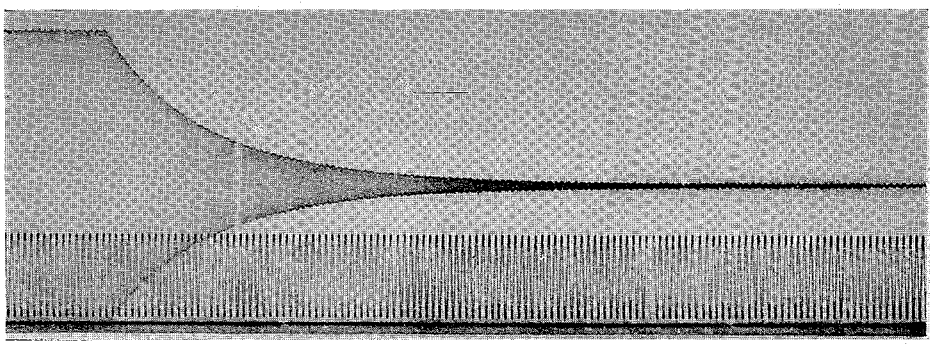

Fig. 42. C 2 ice, No. 208, −20°C, $\rho=0.910$, $E=9.52\times^{10}$, $\tan\delta=0.0049$.

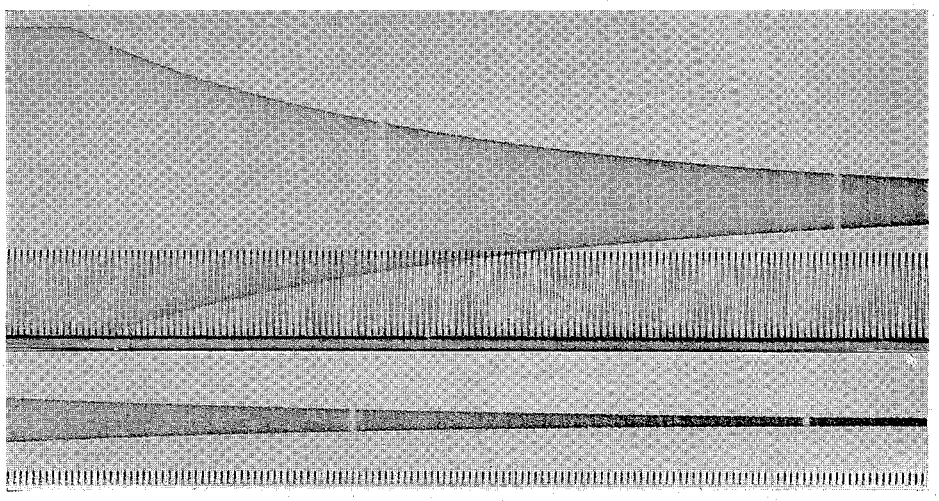

Fig. 43. C 2 ice, No. 209, −30°C, $\rho=0.910$, $E=9.91\times10^{10}$, $\tan\delta=0.0012$.

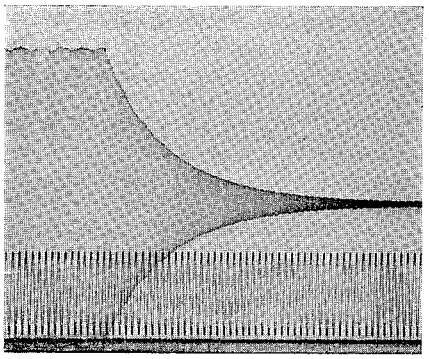

Fig. 44. I ice, No. 208, −20°C, $\rho=0.17$, $E=8.58\times10^{10}$, $\tan\delta=0.0079$.

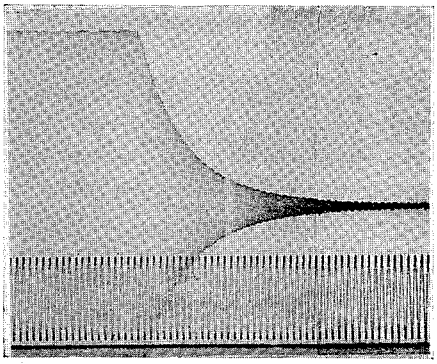

Flg. 45. A 2 ice, No. 208, −20°C. $\rho=0.915$, $E=8.55\times^{10}$, $\tan\delta=0.0106$.

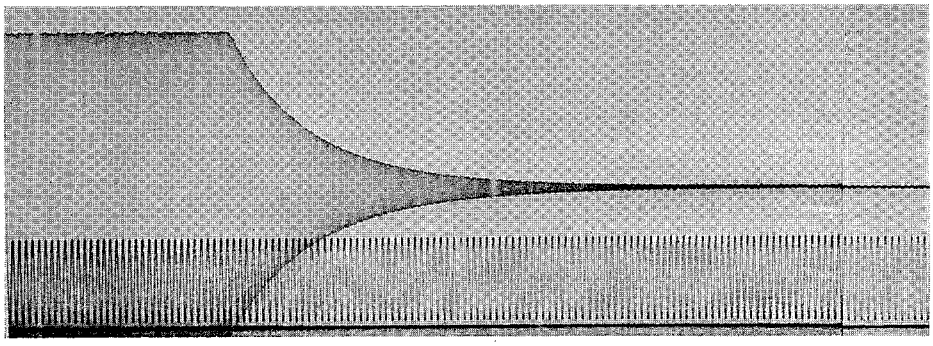

Fig. 46. B 2 ice, No. 208, −20°C, $\rho=0.910$, $E=8.79\times10^{10}$, $\tan\delta=0.0054$.

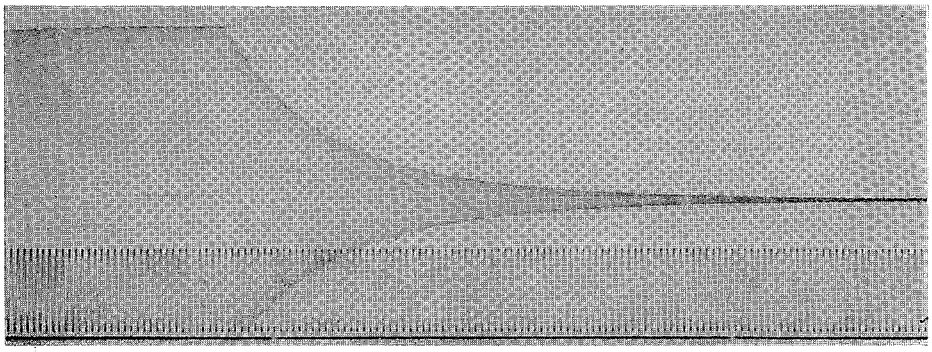

Fig. 47. C 1 ice, No. 208, −20°C, $\rho=0.911$, $E=8.79\times10^{10}$, $\tan\delta=0.0054$.